

Point defect engineering in thin-film solar cells

Ji-Sang Park¹, Sunghyun Kim¹, Zijuan Xie^{1,2} and Aron Walsh^{1,3*}

Abstract | Control of defect processes in photovoltaic materials is essential for realizing high-efficiency solar cells and related optoelectronic devices. Native defects and extrinsic dopants tune the Fermi level and enable semiconducting p–n junctions; however, fundamental limits to doping exist in many compounds. Optical transitions from defect states can enhance photocurrent generation through sub-bandgap absorption; however, these defect states are also often responsible for carrier trapping and non-radiative recombination events that limit the voltage in operating solar cells. Many classes of materials, including metal oxides, chalcogenides and halides, are being examined for next-generation solar energy applications, and each technology faces distinct challenges that could benefit from point defect engineering. Here, we review the evolution in the understanding of point defect behaviour from Si-based photovoltaics to thin-film CdTe and Cu(In,Ga)Se₂ technologies, through to the latest generation of halide perovskite (CH₃NH₃PbI₃) and kesterite (Cu₂ZnSnS₄) devices. We focus on the chemical bonding that underpins the defect chemistry and the atomistic processes associated with the photophysics of charge-carrier generation, trapping and recombination in solar cells. Finally, we outline general principles to enable defect control in complex semiconducting materials.

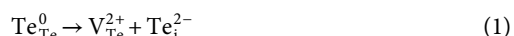
An understanding of defects and defect processes is necessary to enable control of functionality and efficiency in semiconductor devices^{1,2}. For applications in light conversion, including solar cells and solar fuels, photogenerated electrons and holes must have lifetimes sufficient for collection or reaction to occur before recombination. On the one hand, defects in semiconducting materials can limit the transport (that is, the mobility and diffusion length) of charge carriers, but on the other hand, they are important for tuning the carrier concentrations and Fermi level for realizing p-type (hole-conducting) and n-type (electron-conducting) materials. The formation of defects that introduce levels deep (that is, with a thermal activation energy $E \gg k_B T$ from the valence or conduction band edges, where k_B is the Boltzmann constant and T is the temperature) within the bandgap of a photovoltaic semiconductor should generally be avoided. Such levels can form intrinsically or extrinsically and can trap electrons or holes, which decreases the carrier extraction efficiency. Each photovoltaic technology shares the same fundamental principle of light-to-electricity conversion but can exhibit distinct defect processes (TABLE 1).

In this Review, we examine the defect chemistry and physics of a variety of photovoltaic materials, ranging from an elemental semiconductor to multicomponent compound semiconductors and hybrid organic–inorganic compounds (FIG. 1). We link the underlying

crystal structures and chemical bonding to trends in the defect formation energy and concentrations, optical levels and electron–hole recombination rates. We show how the requirements for defect tolerance and control to realize high-efficiency stable photovoltaic devices have evolved from Si to thin-film CdTe and Cu(In,Ga)(S,Se)₂ (CIGS) technologies, through to the latest generation of perovskite and kesterite solar cells.

Classification of point defects

The statistical mechanics of defects in crystalline materials have been studied for almost a century. The atoms in crystalline materials form a regular lattice, but, as was first realized by Frenkel³, at thermal equilibrium a number of atoms will leave their regular sites. Starting from a perfect crystal, such a process creates two point defects — an interstitial defect and the associated atomic vacancy — and these may be in neutral or charged states. Taking the example of CdTe and using the standard notation M_l^q (where M is the species, l is the lattice site and q is the relative charge), the formation of a charged Te Frenkel pair can be written as



where the reactant (left-hand side) represents one occupied Te site in the perfect crystal and the product

¹Thomas Young Centre and Department of Materials, Imperial College London, London, UK.

²Department of Physics, Harbin Institute of Technology, Harbin, China.

³Department of Materials Science and Engineering, Yonsei University, Seoul, South Korea.

*e-mail: a.walsh@imperial.ac.uk

<https://doi.org/10.1038/s41578-018-0026-7>

Table 1 | Comparison of performance and defects in Si and thin-film photovoltaic technologies

Technology	Power conversion efficiency ^a (%)	Doping type	Extrinsic dopants	Common point defects	Lifetime of minority carrier
Si	26.7	n or p	B, P, Al (REF. ¹⁵)	Si dangling bonds, transition metals, B–O complexes	8.8 ms (REF. ⁶²)
CdTe	21.0	n or p	Cu, Cl, P	V _{Cd} , V _{Te} , Te _{Cd} , Te–Te	1–30 ns (REF. ¹¹²)
CIGS	21.7	p	–	V _{Cu} , (In,Ga) _{Cu}	10–100 ns (REF. ²⁴¹)
CZTS	10.0	p	–	V _{Cu} , Zn _{Cu} , Cu _{Zn}	<1 ns (REF. ¹⁸⁵)
Halide perovskite	20.9	n or p	–	V _{Pb} , V _i , V _{MA} , I _i	100–1,000 ns (REFS ^{242–245})

CIGS, Cu(In,Ga)(S,Se)₃; CZTS, Cu₂ZnSn(S,Se)₄; i, interstitial; MA, methylammonium; V, vacancy. ^aThe listed power conversion efficiencies are for the record highest light-to-electricity conversion achieved in a photovoltaic device of at least 1 cm² (REF.⁶⁷).

(right-hand side) corresponds to a positively charged vacancy (V) and interstitial (i) involving the Te anion. Site vacancies and interstitials are two of the most common point defects, in addition to antisites such as the (Cu_{Zn}⁺ + Zn_{Cu}⁺) complex common in Cu₂ZnSnS₄. In the commonly used notation developed by Kröger and Vink, relative effective charges are indicated using dots (positive), dashes (negative) and crosses (neutral); for example, V_{Te}²⁺ ≡ V_{Te}^{..}.

The concentration of a given point defect in a material at equilibrium is determined by the free energy of defect formation (BOX 1), which in turn depends on the chemical potentials of the system, including the growth environment (usually expressed in terms of atomic chemical potentials) and the Fermi level (that is, the electronic chemical potential). The atomic chemical potentials can be controlled by varying the reaction conditions for crystal growth. For example, in the synthesis of CIGS thin films, varying the temperature and partial pressure of sulfur vapours in the synthesis chamber can be used to control the concentration of sulfur vacancies in the material.

The enthalpic cost of point defect formation typically falls in the range 0–10 eV, and defect concentrations range from 10¹²–10²⁰ cm⁻³, with the high end of the range corresponding to about one imperfection in every 100 lattice sites. The defect formation energy can become negative for materials that favour non-stoichiometry, such as copper telluride (Cu_{2-x}Te), which is used as a back electrical contact in some CdTe device architectures. There is a well-developed theoretical framework for calculating the energetics of defect formation, which has evolved from classical simulations⁵ to modern first-principles techniques, including those based on density functional theory (DFT)⁶. A given point defect can exist in a variety of charge states and can transition between them by exchanging electrons or holes with the valence or conduction bands of the semiconductor host. Point defects are categorized as either shallow or deep, depending on where in the bandgap a charge transition level is generated, and as either an acceptor or donor, which is determined by the accessible charge states and the role of the defect in determining the Fermi level (BOX 2).

Point defects are not necessarily static in the lattice but diffuse with a rate that is limited by the activation energy for solid-state diffusion. Ion transport can

proceed according to various mechanisms, including vacancy-mediated and interstitial-mediated diffusion. The self-diffusion coefficient of Si is ~10⁻¹⁶ cm² s⁻¹ (at 1,000 °C), making Si diffusion a slow process⁷. By contrast, Cd diffuses at ~10⁻⁸ cm² s⁻¹ in CdTe (at 1,000 °C)⁸, and Cu diffuses at up to 10⁻⁸ cm² s⁻¹ in CuInSe₂ (at 380 °C)⁹ and at >10⁻⁵ cm² s⁻¹ in Si (at 380 °C), which constitutes a fast diffusion process¹⁰. In a working solar cell, built-in electric fields can further enhance the diffusion rates (that is, ion drift and electromigration) and in severe cases can give rise to hysteresis — that is, a dependence on the history of the device — in the current–voltage response¹¹.

The identification of point defects in materials is challenging owing to their dilute concentrations, which are beyond the resolution of most standard materials characterization techniques (for example, X-ray diffraction). The assignment of particular signals often requires a multi-technique approach with experimental analysis assisted by theory and simulation. Beyond electrical measurements, it is also possible to probe the optical (for example, by measuring photoluminescence and photoconductivity), thermal (for example, using deep-level transient spectroscopy and by measuring thermally stimulated conductivity), vibrational (for example, using infrared and Raman spectroscopy) and magnetic (for example, using electron-spin resonance) responses of point defects. Even in well-studied optoelectronic materials, including ZnO and GaN, the atomic origin of specific defect luminescence features remains the subject of ongoing research and debate¹². Sub-bandgap defect levels have been reported in a range of photovoltaic materials (TABLE 2) and show that for each material the defect levels are widely distributed within the bandgap. As discussed below for each technology, innovative procedures have been developed to avoid the most detrimental of these defects in order to realize efficient light-to-electricity conversion in operating solar cells.

Silicon

Si is one of the most abundant chemical elements. It naturally forms a face-centred cubic diamond structure (space group $Fd\bar{3}m$) (FIG. 1a), with each atom in a tetrahedral coordination environment. Crystalline Si has a strongly indirect bandgap of 1.12 eV at 300 K,

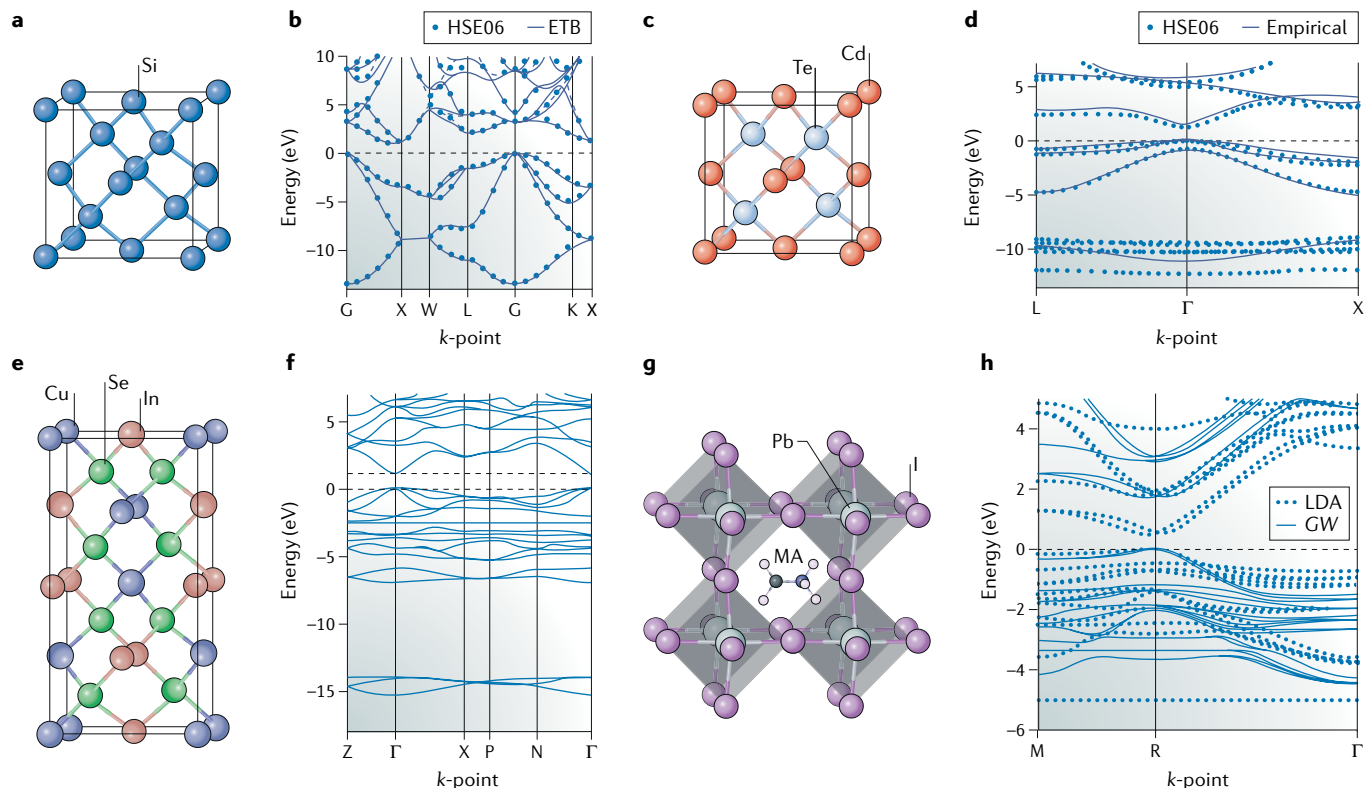


Fig. 1 | Crystal structure and electronic band structure of Si, CdTe, CuInSe₂, and CH₃NH₃PbI₃. **a** | Si adopts a face-centred cubic diamond structure. **b** | Electronic band structure of bulk Si calculated using density functional theory (DFT) with the Heyd-Scuseria-Ernzerhof (HSE06) functional and obtained using an empirical tight-binding (ETB) model. **c** | CdTe adopts a face-centred cubic zinc-blende structure. **d** | Band structure of CdTe calculated using DFT with the HSE06 functional and an empirical non-local pseudopotential scheme. **e** | Conventional unit cell for the chalcopyrite CuInSe₂. **f** | Band structure of CuInSe₂ in the body-centred tetragonal primitive cell calculated using DFT with the HSE06 functional. **g** | Atomic structure of pseudo-cubic methylammonium lead iodide (CH₃NH₃PbI₃). **h** | Quasiparticle self-consistent GW band structure (where G denotes the Green's function and W denotes the screened Coulomb interaction) of CH₃NH₃PbI₃ calculated with the inclusion of spin-orbit coupling. The band structure computed using DFT with the local density approximation (LDA) is shown for comparison. The valence band maximum is set to 0 eV in panels **b**, **d**, **f** and **h**. MA, methylammonium. Panel **b** is adapted with permission from REF.²³⁸, American Physical Society. Panel **d** is adapted with permission from REF.²³⁹, Elsevier. Panel **f** is adapted with permission from REF.²⁴⁰, American Institute of Physics. Panel **h** is adapted with permission from REF.¹⁹², American Physical Society.

with degenerate heavy-hole and light-hole bands and hole effective masses of $0.54m_e$ and $0.15m_e$, respectively (where m_e is the free electron rest mass). Si also features six-fold-degenerate conduction band valleys with an electron effective mass of $0.26m_e$ (REF.¹³) (FIG. 1b). The associated relative dielectric constant is ~12 at room temperature¹³. In tetrahedrally coordinated elemental semiconductors, it is common to describe the bonding in terms of the overlap of the valence s and p atomic orbitals to form sp³ hybrid orbitals, with the valence band composed of bonding combinations and the conduction band consisting of the corresponding antibonding combinations.

Si solar cells are a mature photovoltaic technology^{14,15}, and thus many aspects of point defects have been thoroughly investigated and documented over the past 60 years. In this section, we introduce some essential features of defect engineering in Si photovoltaics, which can be potentially transferred to emerging photovoltaic technologies. For a more comprehensive overview of defect processes in Si, several good reviews are available^{16,17}.

Doping efficiency. To produce effective semiconductor devices, it is necessary to introduce dopants (shallow donors and acceptors) that can generate charge carriers and whose spatial distribution in the device can be controlled. The ability to dope a potential photovoltaic material is crucial as some photovoltaic cell architectures require both n-type and p-type semiconductors to form p–n or p–i–n junctions. Si can be doped with B (an electron acceptor) and P (an electron donor), which are shallow dopants for p-type and n-type behaviour, respectively. Thus, homojunction p–n Si solar cells are readily achieved. Both p-type and n-type Si wafers are available; however, p-type wafers have been more widely used as B has a higher segregation coefficient than P, making it advantageous for obtaining a spatially homogeneous doping profile¹⁵. The diffusivity and diffusion mechanisms of dopants in Si have been thoroughly analysed; for example, the solid-state diffusion of P and Al has been well studied as this method is often used to make n-type and p-type regions, respectively, for single-crystal solar cells¹⁷.

Recombination rates. The rates of electron–hole recombination must be controlled to achieve long charge-carrier lifetimes and thus efficient extraction. There are various recombination processes for photogenerated electrons and holes, which can be classified into three main types: radiative recombination, non-radiative recombination and Auger recombination (BOX 3). The challenge with using Si has been the suppression of non-radiative losses, including defect-induced deep-level (Shockley–Read–Hall) and surface recombination pathways^{18–20}. Radiative and Auger recombination coefficients

are intrinsic properties of a material and are therefore more difficult to modify. Auger recombination becomes significant only at high injection levels (that is, at a high light intensity) for direct bandgap materials. However, owing to the strongly indirect bandgap of Si (and thus the low radiative recombination rate), Auger processes limit the theoretical maximum power conversion efficiency (PCE) to approximately 29% under 1 sun illumination²¹.

It has been necessary to use surface passivation in Si solar cells to reduce surface recombination and realize practical large-area, high-efficiency devices^{19,20}. Low-coordinate Si atoms at the surface have amphoteric dangling bonds (they act as donors in p-type Si and as acceptors in n-type Si) that introduce a half-occupied deep level in the bandgap^{22,23}. These deep levels can be chemically passivated by terminating the Si dangling bonds with H atoms²⁴, which can be achieved through the deposition of a hydrogenated silicon nitride (SiN_x) layer^{15,20} or a hydrogenated amorphous Si layer¹⁴. Further migration of H into the bulk region can neutralize shallow dopants as interstitial H has the ability to act as a compensating donor or acceptor in p-type and n-type Si, respectively²⁵. In addition to chemical passivation with H atoms, surface electron–hole recombination can also be suppressed by using a fixed charge in a dielectric layer to repel one type of carrier and attract the other^{15,26}, thereby decreasing the rate of recombination²⁰.

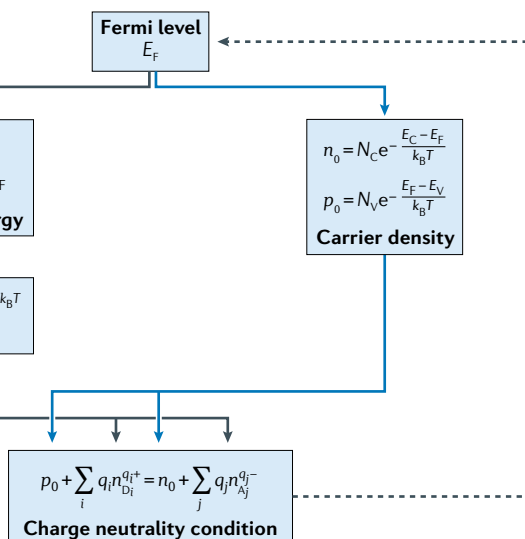
Box 1 | Equilibrium thermodynamics of point defect formation

The thermodynamic driving force for the formation of point defects in crystalline materials is configurational entropy (S). Although perturbing the ordering of atoms in a crystal requires enthalpy (H), the overall free energy of a crystal (G) is lowered by the gain in entropy according to $G = H - TS$. Minimizing the free energy of a crystal with respect to the concentration of a defect (n_i) yields a simple expression: $n_i = N_{\text{site}} g_q \exp(-\Delta H_f/k_B T)$, where N_{site} is the number of lattice sites, g_q is a degeneracy factor (for example, the number of spin configurations) of a charge state q , ΔH_f is the formation enthalpy of the point defect (α), k_B is the Boltzmann constant and T is the temperature.

In atomic calculations of defect formation, it is common to separate ΔH_f into the sum of three components: the total energy change (ΔE) between a pristine and defective crystal, the exchange of n_i elements with a reservoir of atomic chemical potential μ_i and the exchange of q electrons with a reservoir of electronic chemical potential (the Fermi level, E_F).

It becomes more complex to calculate the equilibrium concentration of point defects in an imperfect semiconductor with a range of defects in various charge states. The concentrations of electrons (n_0) and charged acceptors A^- (n_A) must balance the concentration of holes (p_0) and charged donors D^+ (n_D): $p_0 + n_D = n_0 + n_A$. The concentration of carriers is determined by the position of E_F : $n_0 = N_C \exp(-(E_C - E_F)/k_B T)$ and $p_0 = N_V \exp(-(E_F - E_V)/k_B T)$, where N_C and N_V are the effective density of states for the conduction and valence bands, respectively, and E_C and E_V are the energies of the bottom of the conduction band and top of the valence band, respectively.

In modern defect theory, the equilibrium concentrations of charge carriers and defects can be calculated self-consistently by determining the E_F of the system under the constraint of overall charge neutrality (see the schematic below). It has become commonplace to calculate the self-consistent concentration of carriers and defects using first-principles techniques, as implemented, for example, in the SC-FERMI code. However, further advances are needed to incorporate finite-temperature effects (such as vibrational entropy and thermal expansion) and to more realistically simulate experimental growth conditions, including the thermodynamic activity of gases and solvents used in the synthesis of real materials.



Control of unintentional impurities. Controlling unintentional impurities is essential in Si as many common metal contaminants are detrimental to the PCE owing to their deep defect levels^{16,27–29}. The thermal stability of impurities commonly found in Si and their electrical properties have been thoroughly documented^{30–32}. Low-cost solar-grade Si wafers generally have a higher concentration of recombination centres (with a metal concentration <200 parts per billion per weight (ppbw)) than electronics-grade Si (metal concentration <2 ppbw)^{33–36}. The behaviour of transition metals in Si have been the subject of detailed measurements. For first-row transition metals, there is an increase in both solubility and diffusivity on going from Ti to Cu (REFS^{28,29,37,38}). The defect levels of metal impurities have been thoroughly investigated by both spectroscopic methods^{27,29,37,39–43} and quantum mechanical simulations^{44,45}. The most detrimental impurities can be removed from the material using appropriate processing techniques^{33,38,46,47}. Several gettering methods have been developed to reduce the harmful effects of metal impurities on charge carriers by directing impurity segregation (for example, as precipitates on the surface).

Given the long history of Si electronics research, the understanding and assignment of defect processes has evolved over time⁴⁸. The application of high-resolution experimental probes has enabled the identification of specific defects in Si and their physical properties^{49–52}. For example, native defects and their interactions with impurities were extensively studied by electron paramagnetic resonance spectroscopy⁴⁹, and positron annihilation spectroscopy was used to investigate the local structure of vacancy defects⁵⁰. The configuration of O impurities in Si was successfully analysed by vibrational

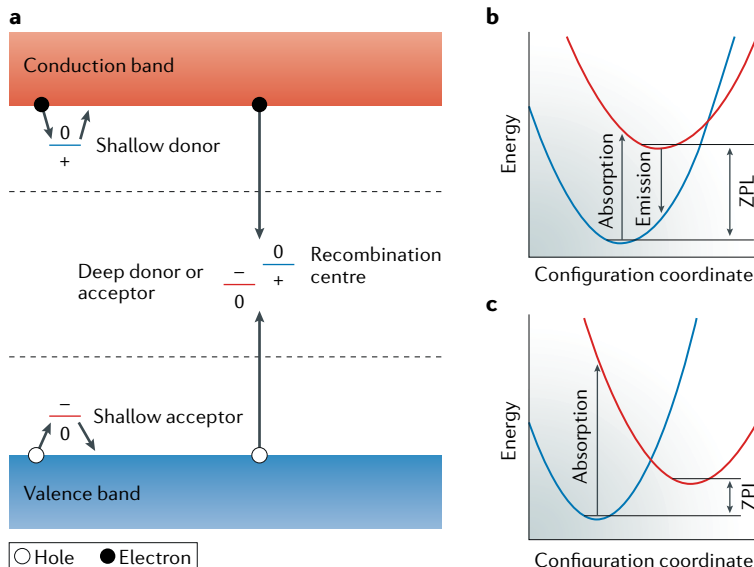
Box 2 | Classification of defect levels in semiconductors

When a Si crystal is doped with P, the system gains an excess electron owing to the higher atomic number of the impurity atom. This excess electron can remain trapped at the substitutional defect site (corresponding to the neutral state of the defect) or be donated to the conduction band of the host material (corresponding to the charged state of the defect) to become a free charge carrier. The energy difference between the charged and neutral states of the defect corresponds to the ionization level for the donation of an electron to the conduction band: $P_{\text{Si}}^0 \rightarrow P_{\text{Si}}^+ + e^-$. For B, which contains one less valence electron than Si, an equivalent acceptor level can be defined with respect to the valence band of the host material: $B_{\text{Si}}^0 \rightarrow B_{\text{Si}}^- + h^+$.

Defects that introduce levels close to the valence or conduction bands are termed shallow. Electronic levels with a thermal activation energy $E < k_B T$ from a band edge (where k_B is the Boltzmann constant and T is the temperature) are effective at generating free charge carriers (see the figure, panel a; blue and red lines represent donor and acceptor ionization levels, respectively). For example, shallow donors favour a positive charge state (+) and donate electrons to the conduction band when the Fermi level is below their ionization level. A defect may also be labelled shallow if the associated electronic wavefunction is delocalized and hydrogenic. Defects that introduce levels deep in the bandgap ($E > k_B T$ from a band edge) can still be ionized optically and can also act as effective intermediate states for the generation of an electron–hole pair or to facilitate electron–hole recombination. Deep levels are often associated with a large lattice distortion and an electronic wavefunction that is localized on a single atom or a small group of atoms. If the defect wavefunction overlaps with the continuum of valence or conduction bands, it is termed a resonant state.

It is important to make a distinction between two types of defect ionization process. Optical defect levels involve fast electronic transitions between two charge states of a defect — that is, a vertical Franck–Condon process with no response in the local atomic structure — caused by the absorption or emission of a photon, as commonly seen in photoluminescence experiments. Thermal defect levels involve a slower transition between two energy minima on a potential energy surface — a process that involves structural relaxation, as described by moving horizontally along the potential energy surface — and are often probed using capacitance-based techniques, such as deep-level transient spectroscopy. The difference between the observable optical and thermal ionization levels for a given point defect is due to the structural relaxation energy.

The potential energy surfaces associated with changing the charge of a point defect are often shown in the form of configuration coordinate diagrams (see the figure, panels b and c), which contain information on both optical absorption and emission processes, as well as the thermal transition in the form of the zero-phonon line (ZPL). The configuration coordinate (x axis) corresponds to the degree of collective local lattice distortion between the configurations of a defect centre with different charge states. Defects with weak coupling to the lattice show a small shift in the ground and excited state potential energy surfaces and can be expected to be active for luminescence (see the figure, panel b). Strong coupling to lattice distortions results in a large shift in the configuration coordinate, suppressing luminescence and promoting non-radiative transitions accompanied by multiphonon (heat) emission to the lattice (see the figure, panel c).



spectroscopy⁵¹, and the concentrations of impurities have also been studied by secondary ion mass spectrometry⁵². Re-evaluation of defect processes using state-of-the-art techniques can sometimes challenge accepted understanding. For example, in the study of Ni diffusivity in Si, the long-accepted value of the solid-state diffusion barrier was re-assessed in 2013 by measuring the accumulation of Ni impurities on the Si surface. Using this approach, the value of the solid-state diffusion barrier was estimated to be 0.15 eV, which is much lower than the previous value of 0.47 eV and more consistent with the calculated value of 0.21 eV (REF. ⁵³). From a theoretical perspective, most initial simulations of defects in Si relied on approximate methods. The first wave of DFT calculations were based on the local density approximation (LDA) and suffered from large errors in the structures and bandgaps, which required a posteriori correction schemes. The fundamental properties of point and complex defects are being revisited using advanced methods, including hybrid DFT functionals, which incorporate a fraction of exact Hartree–Fock exchange to address electron self-interaction, and many-body GW theory (where G denotes the Green's function and W denotes the screened Coulomb interaction) to include quasiparticle excitations. These advanced methods reduce bandgap underestimation errors and thus enable calculated defect levels to be directly compared with measured values^{45,54}. Recent studies have further shown that migration barriers for defect diffusion in Si can be predicted with smaller errors using recently developed DFT exchange–correlation functionals^{45,55,56}.

Device ageing and lifetime. The decrease in the performance of operating solar cells over long timescales is often attributable to degradation processes involving chemical impurities and point defects. In particular, light-induced degradation (LID) and potential-induced degradation (PID) are two of the processes most detrimental to the long-term performance of solar cells. Si-based solar cells have already achieved high PCE in large-area devices, and thus control of the defects responsible for device ageing is of key importance.

A well-documented degradation mechanism is B–O LID, which is mainly observed in B-doped Czochralski (cz)-grown Si (REFS^{57–59}). Defect pairs composed of B and O form over time and introduce deep levels in the bandgap that act as efficient non-radiative recombination centres. Typical cz-Si samples contain O impurities at a concentration of $\sim 10^{18} \text{ cm}^{-3}$, which is higher than float-zone Si that is not manufactured using quartz crucibles. Different models have been suggested and examined to explain the degradation phenomena; however, there is no consensus on the underlying atomistic process^{57–59}. Substitution of Ga for B is found to be beneficial, but Ga has a lower segregation coefficient than B in Si (REF.⁵⁷). Many high-efficiency Si solar cells are now based on n-type Si (REF.^{60–62}), which is free from the B–O LID pathway⁵⁷.

Although B–O LID is most commonly observed, LID can also be caused by extrinsic Cu impurities in the form of substitutional Cu ions and/or precipitated Cu clusters⁵⁷. Cu-induced LID can be prevented by

Table 2 | Sub-bandgap defect levels in a range of photovoltaic materials

Technology	Defect	Ionization levels (eV)	Experimental or calculated?	Refs
Si	Si dangling bonds	0.31 (1+/0), 0.80 (0/1−)	Expt.	²⁴⁶
	V_{Si}	0.08 (2+/0), 0.91 (0/2−)	Calc.	⁵⁶
	B–O complexes	−0.34, −0.38, −0.41 (donor)	Expt.	^{59,247–249}
		0.24, 0.26, 0.28, 0.31 (acceptor)		
CdTe	Cu_{Si}	0.20 (1+/0), 0.54 (0/1−), 0.97 (1−/2−)	Calc.	⁴⁵
	V_{Cd}	0.35 (0/2−)	Calc. ^a	⁷⁹
	Te_{Cd}	0.50 (2+/0), 1.29 (0/2−)	Calc. ^a	⁷⁹
	Cl_{Te}	1.3 (1+/0)	Calc. ^a	⁷⁸
	Unclassified	0.12, 0.14, 0.15, 0.20, 0.25, 0.32, 0.43, 0.57, 0.76, −0.64, −0.79, −1.10	Expt.	⁹⁶
CIGS	V_{Cu}	0.08 (0/1−)	Calc.	²⁵⁰
	In_{Cu}	0.86 (2+/0)	Calc.	²⁵⁰
	V_{Se}	0.30 (2+/0)	Calc.	²⁵⁰
		0.08 (2+/0), 0.98 (0/1−)	Calc.	¹²⁷
	$V_{Se}–V_{Cu}$	0.29 (1+/−), 0.86 (1−/2−)	Calc.	¹²⁷
	Unclassified	0.6, 0.81, 0.1–0.4, 0.45–0.58, 0.33, 0.3, 0.07	Expt.	²⁵¹
Halide perovskite	I_i	0.15 (0/1−), 0.58 (1+/1−), 1.01 (1+/0)	Calc. ^{a,b}	²⁰³
	I_{MA}	0.17 (1−/2−), 0.53 (0/2−), 0.91 (0/1−)	Calc. ^{a,b}	²⁰³
	Unclassified	−0.46, −0.78, −0.82	Expt. ^c	²⁰⁰

The sign of an ionization level indicates whether it is referenced with respect to the energy of the valence band maximum (positive value) or conduction band minimum (negative value) of the pristine host material. Calc., calculated values; CIGS, Cu(In,Ga)(S,Se); Expt., experimentally determined values; i, interstitial; MA, methylammonium; V, vacancy. ^aValues of ionization energies reported here are estimated from plots of the calculated data.

^bMethylammonium lead bromide. ^cFormamidinium lead iodide with a small fraction of methylammonium lead bromide (~5 mol%).

depositing negative corona charges on the surface of a wafer to attract the positively charged Cu ions to the surface and subsequent etching of the Cu-rich surface layer⁶³.

Na-contaminated stacking faults have been linked to a PID of the shunting type. Na^+ ions drift from soda-lime glass or the surface of SiN_x towards the SiN_x/Si interface owing to the built-in electric field, and such Na^+ -contaminated stacking faults typically form during long-term device operation⁶⁴. Contaminated stacking faults can serve as channels for charge-carrier transport, resulting in reduced shunt resistance, which lowers the PCE (as a result of the lower voltage and fill factor) of a solar cell. The degraded cells can be partially regenerated by out-diffusion of Na^+ from the interface, which can be driven thermally or by the application of a reverse-bias voltage⁶⁴. The degradation rate can be decreased by using a SiN_x dielectric layer with small values of x that neutralizes Na^+ ions or by substituting soda-lime glass with other glass compositions that contain less Na (REF⁶⁴).

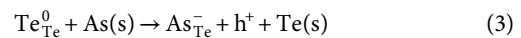
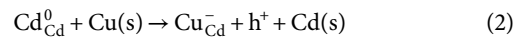
Cadmium telluride

Since CdTe was theoretically proposed in 1956 to have a higher PCE than Si owing to its more optimal bandgap for single-junction solar cells⁶⁵, significant efforts have been made to design and optimize cell architectures⁶⁶. In 2016, the company First Solar reported a CdTe solar cell with a PCE of 22.1%⁶⁷. The module efficiency of large-aperture-area (~7,000 cm²) devices is as high as 18.6%⁶⁷, which has enabled the successful commercialization of this technology.

CdTe is a semiconducting compound that adopts the zinc-blende face-centred cubic crystal structure (space group $F\bar{4}3m$) (FIG. 1c). CdTe has a direct bandgap of 1.48 eV at 300 K, with electron and hole effective masses < 0.15 m_e , making it suitable for single-junction solar cell applications¹³ (FIG. 1d). The formal valence electronic configuration of Cd^{2+} ($4d^{10}5s^0$) and Te^{2-} ($5s^25p^6$) suggest an upper valence band formed of Te 5p orbitals and a lower conduction band formed of Cd 5s orbitals, as found in band structure calculations⁶⁸. In contrast to Si, the polarity of the Cd–Te bond results in optically active phonon modes above 4 THz and a significant difference between the high-frequency relative dielectric constant of 7.1 and the low-frequency (or static) relative dielectric constant of 10.4.

Doping efficiency. CdTe solar cells have problems associated with their defect physics that are more fundamental than in Si solar cells; in particular, these problems are related to low doping efficiency and high non-radiative electron–hole recombination rates^{69–75}. Currently, the best CdTe devices are based on a p-type CdTe/n-type CdS heterojunction. The hole concentration in p-type CdTe needs to be sufficient to support a high cell voltage, but this has proved difficult to achieve in CdTe thin films. The dominant intrinsic acceptor defect in CdTe is the Cd vacancy (V_{Cd}), and the associated acceptor level is deep at ~0.4 eV higher than the valence band edge according to hybrid DFT (with the Heyd–Scuseria–Ernzerhof (HSE) functional) calculations^{75–78} (FIG. 2). Higher concentrations of the ionized Cd vacancy defect can, in principle, be achieved if CdTe is grown under Cd-poor and Te-rich conditions and can be further enhanced if the layer is grown at high temperature and subsequently quenched to room temperature⁷⁹. The formation energies of defects with different charge states were used to estimate the net hole concentration in CdTe under different growth conditions; the net hole concentration is limited to ~10¹⁵ cm^{−3} unless there are additional dopants present⁷⁵. Extrinsic acceptor dopants are therefore necessary to increase the concentration of holes in p-type CdTe.

Obvious candidates for p-type doping are group 1 or group 11 elements that can substitute for Cd and group 15 elements that can substitute for Te (REFS^{80,81}), as exemplified in equations 2 and 3, respectively.



Experimentally, doping with group 11 elements has been explored, including the use of Cu as an acceptor in CdTe (REF.⁸²). The formation energy of the Cu_{Cd} defect is sufficiently low to achieve high concentrations, and its acceptor level is found to be shallower than that of V_{Cd}; thus ionization is more efficient^{75,78}. Cu impurities can be incorporated in the form of interstitials that act as electron donors, and the concentration of impurities can be modulated by controlling the atomic chemical

potentials⁷⁵. However, as the Cu concentration increases, Cu_{Cd} defects can capture a significant number of minority electron carriers (the capture cross section of Cu_{Cd} is $\sim 10^{-16} \text{ cm}^{-2}$)⁸³⁻⁸⁵. Therefore, the concentration and doping profile of Cu_{Cd} should be carefully controlled⁷⁰ on the basis of knowledge of the diffusion mechanism and pathways⁸⁶. Group 1 elements can also be used to enhance hole concentrations when CdTe is grown under Te-rich conditions (as opposed to Cd-rich conditions) owing to the increased preference for the substitutional form over interstitials⁷⁵.

Doping with group 15 elements (P and As) has also been attempted experimentally⁷³ as they can introduce shallow acceptor levels when coordinated tetrahedrally^{75,87}. Moreover, this approach has attracted recent attention because a new acceptor source is required for materials grown under Cd-rich conditions to maintain long minority-carrier (that is, electron) lifetimes⁶⁹, as described below. However, it has been predicted that P_{Te} and As_{Te} can transform into deep donors, termed AX centres, that act to limit the doping efficiency^{75,87}. The AX centre is an acceptor analogue of the more common DX centre, which was once thought to be a complex involving a donor (D) and an unknown defect (X) but was later understood to be associated with the structural transformation of an isolated defect⁸⁸. The formation of an AX centre involves the breaking of a Cd–Te bond and an A–Te bond (where A = P or As) and the formation of a new bond between the impurity and a neighbouring Te atom. An AX centre thus forms when the gain in electronic energy is greater than the energy cost to break the bonds^{75,87}. Self-compensation — that is, the spontaneous conversion of an acceptor into a donor — can be partly overcome by non-equilibrium growth, and a hole density as high as 10^{17} cm^{-3} was predicted to be achievable under certain conditions^{75,87}.

Charge-carrier lifetime. In addition to the problem of doping efficiency, the short lifetime of minority charge carriers is another key issue in CdTe solar cells. The lifetime of photogenerated electrons and holes, which takes into account all types of recombination processes, is an important material parameter to optimize in order to achieve high-efficiency devices. Time-resolved photoluminescence (TRPL) measurements have shown that the cell voltage generally increases with charge-carrier lifetime in CdTe devices⁸⁴. DFT calculations (using the generalized-gradient approximation with the Perdew–Burke–Ernzerhof (PBE) functional) suggested that the Te vacancy (V_{Te}) acts as the primary recombination centre^{71,89}. The formation of Te vacancies can be suppressed when the CdTe absorber layer is grown under Te-rich conditions. However, two-photon excitation TRPL measurements indicate that carrier lifetime is longer in CdTe grown under Cd-rich conditions⁶⁹. Bulk recombination can be more accurately captured by two-photon excitation than one-photon excitation as one-photon-excitation TRPL is sensitive to surface recombination^{69,84,90}. Hybrid DFT (with the HSE functional) calculations helped to resolve this contradiction, confirming V_{Te} to

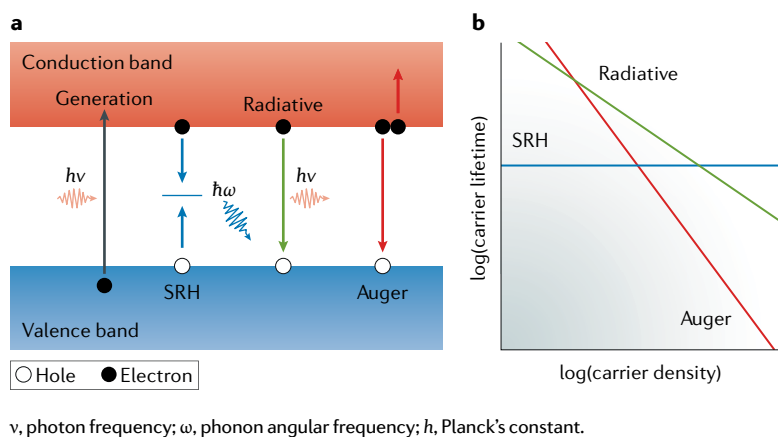
Box 3 | Electron–hole recombination in solar cells

When a semiconductor interacts with light, photons with an energy greater than the bandgap can excite an electron from the valence band into the conduction band, thereby generating an exciton that dissociates into a free electron–hole pair (see the figure, ‘Generation’ in panel a). The photogenerated electrons and holes that are collected at the p–n junction produce the current in a photovoltaic device. Therefore, carrier lifetime is an important parameter that determines the performance of solar cells. Carrier lifetime is limited by the rate of electron–hole recombination, which can be radiative (with light emission) or non-radiative (with only phonon emission). The kinetics of the decay in the concentration of photogenerated charge carriers (n) is often modelled using a third-order rate equation of the form $dn/dt = G - k_1 n - k_2 n^2 - k_3 n^3$, where the charge–carrier generation rate (G) is offset by one-particle (k_1), two-particle (k_2) and three-particle (k_3) recombination processes. The contribution from each process to the total recombination is sensitive to the carrier density and thus the illumination intensity (see the figure, panel b for a typical example).

In a low carrier density regime ($n < 10^{15} \text{ cm}^{-3}$), deep-level non-radiative recombination is often the dominant recombination mechanism. A deep level in the bandgap of a semiconductor provides an intermediate state that facilitates the sequential capture of minority and majority carriers, which can be described by Shockley–Read–Hall (SRH) statistics. The recombination effectively becomes a first-order process (k_1) as the kinetics are usually limited by the capture of the minority carrier. During the recombination process, which may occur in the bulk material as well as at surfaces or interfaces, the energy is dissipated by emitting heat in the form of phonons (lattice vibrations; see the figure, ‘SRH’ in panel a).

At intermediate carrier densities, two-particle band-to-band recombination (k_2) processes, in which photogenerated electrons and holes recombine directly by emitting photons, become important (see the figure, ‘Radiative’ in panel a). This is an unavoidable thermodynamic loss required by the symmetry of light absorption and emission. For valence-to-conduction band recombination, the emitted photons can be re-absorbed by the material, and the process is termed photon recycling. For indirect bandgap semiconductors, the values of k_2 are smaller than those for direct bandgap materials, which places increased weight on k_1 and k_3 processes.

In Auger recombination, a carrier collides with a second carrier of the same type (see the figure, ‘Auger’ in panel a). Following the collision, one carrier gains kinetic energy and is excited to a higher energy state, while the other carrier recombines with a third carrier of the opposite type. As three particles are involved, Auger recombination (k_3) generally limits the carrier lifetime significantly only in a very high carrier density regime ($n > 10^{17} \text{ cm}^{-3}$), but in the case of high-quality (low defect density) Si, it is a limiting process under solar illumination.



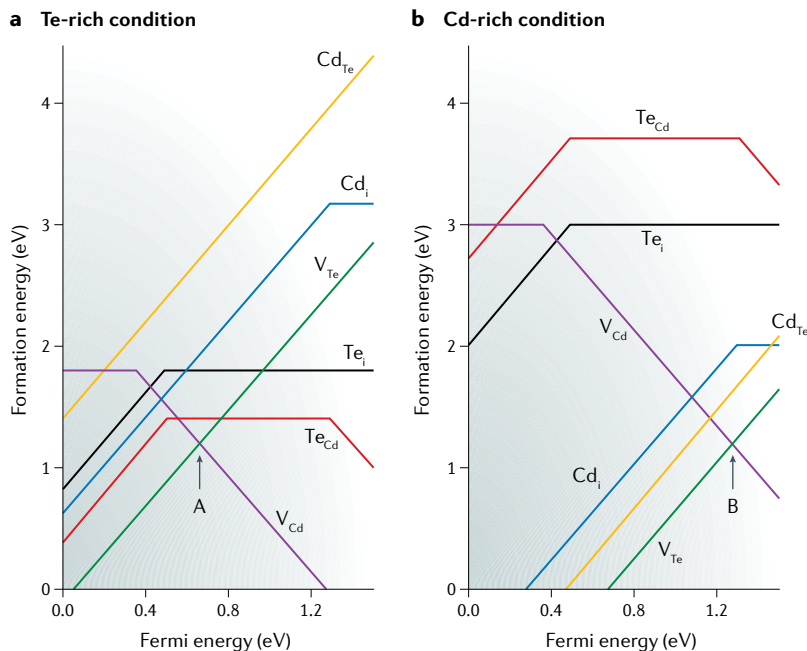


Fig. 2 | Formation energy of intrinsic point defects in CdTe under different growth conditions. The formation energy of intrinsic point defects is dependent on whether CdTe is grown under Te-rich (panel a) or Cd-rich (panel b) conditions. Only the most stable charge states of each defect are shown for clarity. The points A and B denote the predicted Fermi-level pinning energies under equilibrium growth conditions. The deep acceptor level of the Cd vacancy (V_{Cd}) and the low formation energy of the Te vacancy (V_{Te}) make it difficult to achieve p-type CdTe with a high hole concentration. The subscript i indicates an interstitial. Adapted with permission from REF.⁷⁹, American Physical Society.

be a shallow defect and revealing that the Te antisite defect (Te_{Cd}) is the deep-level recombination centre to be avoided^{69,75}. This series of studies again emphasizes that defects should be examined by computational methods that are free from large bandgap and delocalization errors. Deep levels in CdTe are well documented experimentally^{91–96}; however, the atomistic origins of many point defects remain unassigned, and the measured values vary considerably between samples⁹³.

Extended defects. If electron–hole recombination is sufficiently reduced in the bulk material, then suppressing recombination at extended defects (that is, grain boundaries, surfaces and interfaces) becomes essential to further improve the performance of CdTe solar cells^{74,97}. It has been shown that the velocity of surface recombination is higher at Te-rich surfaces than at stoichiometric or Cd-rich surfaces. Dangling bonds and/or dimerized (Te–Te) bonds that violate the octet rule have been suspected to be the origin of the faster surface recombination⁷², and the same bonding features can also form at extended defects^{75,98–100}. In polycrystalline semiconductors, grain boundaries generally decrease the PCE because of their role in fast non-radiative recombination¹⁰¹; however, polycrystalline CdTe solar cells exhibit higher solar conversion efficiencies than monocrystalline CdTe solar cells^{99,102–104}. Grain boundaries can exist in a wide variety of forms, but certain configurations have lower formation energies¹⁰⁵. Theoretical studies suggest that deep levels formed at grain boundaries act as recombination

centres^{105,106}, showing an atomistic similarity to Te_{Cd} antisite point defects^{69,107}.

Chloride treatment, typically with $CdCl_2$, has been widely used to activate CdTe, but the microscopic processes responsible for this activation are still under debate, and there are a number of proposed models^{108–110}. $CdCl_2$ treatment increases carrier lifetimes^{90,101,111,112}, which may originate from the passivation of interface states^{82,113} and/or grain boundaries^{100,106}, band bending at grain boundaries^{99,102}, elimination of deep levels^{94,114} and removal of stacking faults^{110,115}. Recently, using 3D two-photon-excitation TRPL, chloride treatment was shown to reduce surface, interface and grain boundary recombination⁹⁰. Consistent with these findings, when small-grain polycrystalline CdTe is treated with $CdCl_2$, there is an increase in the carrier lifetime, which could be attributable to band bending at grain boundaries^{99,102} or the passivation of grain boundaries by impurity segregation¹⁰⁶. By contrast, large-grain polycrystalline CdTe, which contains a lower density of grain boundaries than small-grain CdTe, was found to have long carrier lifetimes¹¹², even in the absence of $CdCl_2$ treatment. In one model, Cl^- ions segregate to the grain boundaries and form Cl_{Te} defects that donate one electron to either the conduction band (producing free carriers) or deep bandgap states (producing trapped carriers) and become positively charged⁹⁹. Such positively charged ions bend the electronic bands, forming local p–n junctions, and thus charge separation is enhanced.

The detrimental effects of grain boundaries can be passivated by the incorporation of both Cu and Cl impurities¹⁰⁶. The incorporation of S impurities can have a similarly beneficial role as shown by the increase in charge-carrier lifetime near a CdTe/CdS junction⁹⁰, where the S concentration is higher owing to interdiffusion^{116–118}. These additional S atoms mostly reside at the grain boundaries¹¹¹, resulting in S–S or atomically mismatched S–Te bonds that induce a shallower antibonding level than Te–Te bonds¹⁰⁰.

Treatment with $MgCl_2$ has been suggested as an alternative to $CdCl_2$ to reduce the cost and the negative environmental effects of the chloride treatment process¹¹⁹; however, $CdCl_2$ has a smaller bond dissociation energy, and thus, when using this precursor, Cl is more readily incorporated into CdTe (REF.¹¹⁸).

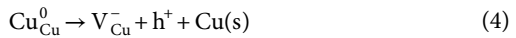
Chalcopyrites

Following the single component (Si) and dual component (CdTe) materials, $CuInSe_2$ is a ternary semiconductor that also adopts a diamond-related crystal structure (FIG. 1e). The chalcopyrite mineral structure features approximately tetrahedral local coordination environments, but the tetragonal lattice (space group $I\bar{4}2d$) allows for additional internal distortions of the Se atoms (resulting in crystal field splitting of the electronic bands). The formal valence electronic configuration of Cu^+ ($3d^{10}4s^0$), In^{3+} ($5s^05p^0$) and Se^{2-} ($4s^24p^6$) suggests an upper valence band formed of Cu $3d$ and Se $4p$ orbitals, and a lower conduction band formed of In $5s$ and Cu $4s$ orbitals (FIG. 1f), as found in early band structure calculations¹²⁰. $CuInSe_2$ has a bandgap of 1.01 eV at 300 K, but often a CIGS solid solution is used to tune the optical

response: chemical substitution of In by Ga (and Se by S) widens the bandgap. The relative dielectric constants of CuInSe₂ are 8.5 (9.5 $\perp c$) at high frequency and 15.2 (16.0 $\perp c$) at the static limit, which are ~20% larger than those of Si and CdTe (REF.¹³).

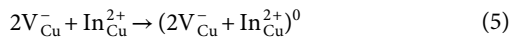
CIGS-based devices are another promising thin-film solar cell technology that is currently available on the market¹²¹. A PCE exceeding 20% has been achieved by careful defect process engineering. As a multicomponent system, the defect physics of CIGS are more complicated than for Si or CdTe, and the direct assignment of electronic and optical signatures to specific point defects becomes even more difficult.

CIGS thin films are self-doped to be p-type by intrinsic defects and thus do not require extrinsic impurities, such as B and P, as used in Si. The Cu vacancy (V_{Cu}), equation 4, is responsible for p-type doping, and the associated acceptor level is shallow, with a low formation energy^{122–125}.



Recent calculations^{126,127} highlighted that Cu antisites (Cu_{In} and Cu_{Ga}) may also substantially contribute to p-type doping. Although $\text{Cu}_{(\text{In},\text{Ga})}$ is predicted to be a deeper acceptor than V_{Cu} , $\text{Cu}_{(\text{In},\text{Ga})}$ is expected to be more abundant for materials processed under Cu-rich conditions.

Isolated In_{Cu} and Ga_{Cu} antisite defects have deep donor levels in the bandgap that can trap minority carriers (electrons)^{123,124}. A high concentration of traps serves to reduce carrier mobility and increase the recombination rate (BOX 2). However, it was experimentally shown that CIGS exhibits excellent electronic properties even when the composition is highly off-stoichiometric^{128,129}. The high defect tolerance of CIGS, which is largely attributable to defect–defect interactions, makes it possible to synthesize active CIGS thin films over a large compositional range of Cu:(In + Ga) from 0.7 to 1.0; several models have been proposed to explain this defect tolerance. The formation of defect complexes involving In_{Cu} and V_{Cu} has been predicted to remove deep levels in the bandgap^{123,124}. The high binding energy of these defect complexes indicates that V_{Cu} tends to form aggregates with antisite defects, turning the deep donors into electrically benign defect complexes, such as in equation 5.



Under grossly off-stoichiometric conditions, defect complexes give rise to the formation of n-type ordered defect compounds (ODCs) at the near surface region^{123,124}. The CIGS/ODC interface forms a high-quality p–n heterojunction¹³⁰. The good lattice match between CIGS and an off-stoichiometric ODC prevents carrier traps from forming at the interface. The electronic band alignment does not produce a barrier to electron extraction and serves to maximize the cell voltage. Thus, the favourable optoelectronic properties of non-stoichiometric CIGS can be attributed to the formation of an ODC. However, in a recent hybrid DFT study¹²⁷, the binding energy of $(2V_{\text{Cu}}^- + \text{In}_{\text{Cu}}^{2+})^0$ was calculated to be only 0.3 eV, which is smaller than in previous reports, and it

was argued that this binding energy is not large enough to be responsible for the defect tolerance. Instead, it was suggested that it is a shallow donor level of In_{Cu} that results in the defect tolerance of CIGS. More sophisticated models that describe the formation of defect clusters beyond the dilute limit, in addition to accounting for the kinetics of defect diffusion and complexation (for example, using Monte Carlo techniques), are needed on this topic.

Defect complexes are also responsible for light-induced and voltage-bias-induced metastability in CIGS. The voltage and capacitance of CIGS solar cells increases under illumination with long-wavelength light^{131–133}. The application of a reverse-bias voltage leads to a similar effect^{134,135}. These changes are explained by a metastable increase in the net acceptor concentration. By contrast, illumination with short-wavelength light leads to the opposite effect of a decreased net acceptor density¹³⁶. It has been proposed that a (partial Schottky) defect complex of $V_{\text{Se}}^-V_{\text{Cu}}$ is the origin of the light-induced and bias-induced metastability¹³⁷. The $V_{\text{Se}}^-V_{\text{Cu}}$ complex exhibits amphoteric behaviour, acting as either a donor or acceptor depending on the position of the Fermi level in the bandgap. Persistent electron (hole) capture converts the $V_{\text{Se}}^-V_{\text{Cu}}$ complex from a shallow donor (acceptor) into a shallow acceptor (donor), accompanying the metastable change in atomic configuration.

Antisite defects, such as Ga_{Cu} in CIGS, have also been identified as metastable defects that limit cell voltage. In III–V and II–VI semiconductors, such as GaAs and ZnSe, respectively, certain extrinsic donors form DX centres — that is, defects that capture rather than donate electrons — which is usually triggered by large structural distortions^{138–140}. In CIGS, intrinsic DX-like behaviour is associated with Ga_{Cu} capturing an electron¹⁴¹. Optical absorption facilitates carrier capture and recombination with structural relaxation. Electron trapping and non-radiative recombination at DX centres are responsible for a drop in the PCE, which is more significant in Ga-rich CIGS.

Increased p-type conductivity has been observed in CIGS containing alkali metals such as Na and K (REFS^{142–145}). The origin for the increased p-type conductivity is attributed to a variety of point defects and the passivation of grain boundaries. Based on DFT calculations¹⁴⁶, it was proposed that the incorporation of Na prevents the formation of In_{Cu} antisites by forming Na_{Cu} and thereby increases the hole concentration. Na antisites, $\text{Na}_{(\text{In},\text{Ga})}$, however, can act as electron acceptors¹⁴², although $\text{Na}_{(\text{In},\text{Ga})}$ are not likely to contribute to the increased hole concentration owing to their high formation energies^{146–148}. Na and K also tend to segregate to the grain boundaries and passivate donor defects^{149,150}.

Similar to CdTe solar cells, much attention has been devoted to the understanding of grain boundaries in CIGS^{151–155}. Studies suggest that Cu-deficient grain boundaries act as barriers for hole transport as the energy of the valence band edge is lowered^{151,155} and that deep levels of octet-rule-violating bonds in grain boundaries can be passivated by the segregation of defects¹⁵⁴. Segregated charged defects in the grain

boundaries modify the long-range electrostatic potential within a grain and cause electronic band bending¹⁵². High concentrations of Cu_{In} and In_{Cu} antisites have also been measured within highly confined regions of <1 nm from the grain boundaries¹⁵³.

Kesterites

I₂-II-IV-VI₄ quaternary semiconductors are a natural extension of II-VI (zinc-blende) and I-III-VI₂ (chalcopyrites) to more complex compounds, as explored in the early work of Goodman¹⁵⁶ and Pamplin^{157,158} and later using DFT-based screening procedures^{79,159,160}. The crystal structure adopted by many of these compounds is based on the kesterite mineral (space group *I*4) with a specific arrangement of the I, II and IV cations on a diamond lattice that involves the spontaneous ordering of alternating cation layers in (201) planes, in which valence II and IV cations occupy valence III cation sites in the chalcopyrite structure¹⁵⁹. Kesterites share many similarities to chalcopyrites in terms of chemical bonding, physical properties and photovoltaic device architectures. The principal advantage of kesterites over chalcopyrites is the replacement of In and Ga by the more sustainable (that is, lower cost and more abundant) elements Zn and Sn. The bandgap of the kesterite Cu₂ZnSnS₄ (CZTS) is ~1.5 eV at room temperature and can be lowered to 1.0 eV by alloying with Se to form Cu₂ZnSnSe₄ (CZTSe)¹⁶¹.

The performance of kesterite solar cells is currently limited by a low open-circuit voltage¹⁶². The current highest record PCE of 12.6%¹⁶³ for kesterite solar cells is still below commercially competitive levels (15–20%). The possible origins of the low performance and voltage deficit are bandgap fluctuations, which reduce the effective bandgap; poor electrical contacts between CZTS and the Mo (back) or CdS (front) buffer layer, which result in rapid electron-hole recombination; and deep-level defects, which act as non-radiative recombination centres in the bulk material¹⁶⁴.

Defect formation in quaternary compounds such as CZTS is highly sensitive to the atomic chemical potentials (that is, the growth conditions), and there are four elements (three cations) for which this property needs to be controlled^{165–169} [FIG. 3]. As the Cu, Zn and Sn cations have similar coordination environments, the energy required to disorder the cation sublattice is low. The existence of secondary phases, such as ZnS and Cu₂SnS₃, limits the choice of growth conditions to avoid harmful defects, such as deep donors. The chemical potentials need to be adjusted carefully to form phase-pure CZTS and to prevent the simultaneous formation of detrimental secondary phases and defects. Under Cu-rich conditions, highly conductive Cu₂S may form and electrically short the device. The Zn-rich phase ZnS has a wide bandgap, which reduces absorption and hinders current collection. Zn-poor conditions lead to the formation of Cu₂SnS₃, which has a smaller bandgap than CZTS¹⁷⁰. The volatile nature of Sn and S means that tin sulfide (SnS and/or SnS₂) evaporates during the sulfurization process, leaving Sn-poor secondary compounds, such as Cu₂S and ZnS.

The remaining SnS and/or SnS₂ may also contribute to a high carrier recombination rate¹⁷¹. Owing to the narrow phase stability field of CZTS and the existence of rich secondary phases and defects, it is difficult to achieve high-quality CZTS crystals or films. The associated structural and electronic inhomogeneity results in poor device performance relative to the theoretical maximum PCE.

In CZTS, there are two competing acceptors, Cu_{Zn} and V_{Cu}, which are formed in Cu-rich or Cu-poor conditions, respectively^{165,166,169}. The acceptor level of Cu_{Zn} is deeper than that of V_{Cu}. However, the lower formation energy of Cu_{Zn} indicates that its concentration is higher than that of V_{Cu}. Therefore, under Cu-rich conditions, Cu_{Zn} contributes more significantly to hole-carrier concentrations, whereas V_{Cu} is responsible for hole-carrier concentrations under Cu-poor conditions. The abundance of Cu_{Zn} and V_{Cu} makes CZTS an intrinsic p-type semiconductor. As the acceptors form spontaneously when the Fermi level is high in energy (close to the conduction band edge), it is difficult to realize n-type CZTS^{165–167}.

Compared with CIGS, CZTS has a greater number of possible antisite defects, because the group 13 elements (In and Ga) in CIGS are replaced by group 12 (Zn) and group 14 (Sn) elements in CZTS. As the differences in the size and valence electron configuration of the Zn and Cu cations are small, it is also easier for the antisite Zn_{Cu} to form than the Cu_{In} and Cu_{Ga} antisites in CIGS^{165–167}. Although it is difficult to distinguish between Cu and Zn using standard X-ray diffraction techniques, neutron diffraction has provided direct confirmation of site disorder in the Cu/Zn sublattice of kesterites¹⁷². Similarly, other charge-compensated defect complexes, such as V_{Cu}-Zn_{Cu}, V_{Zn}-Sn_{Zn} and Cu_{Sn}-Sn_{Cu}, are easy to form, and there is some experimental evidence of their presence^{173,174}. Similar to those in CIGS, charge-neutral defect complexes are expected to passivate deep donor levels and to decrease hole-carrier concentrations in CZTS^{165–167}.

CZTS exhibits a structural transition in the Cu/Zn sublattice at a critical temperature of ~200 °C [REFS^{172,173–181}]. The transition has been attributed to cation disorder, mainly Cu and Zn locating at the 2c and 2d Wyckoff positions of the kesterite structure, respectively. DFT calculations predict that a large number of the antisite defects form as a result of the low formation energies^{165–167}. Monte Carlo simulations showed that the disordered cations form a cluster, which leads to compositional inhomogeneity¹⁸². This inhomogeneity results in bandgap fluctuations, which may contribute to the large voltage deficit in kesterite solar cells. It has been predicted¹⁸¹ that this disorder introduces spatial bandgap fluctuations in the range of several hundred meV. However, in a recent study, the effect of disorder on efficiency was questioned¹⁶⁴. It was claimed that disorder decreases the cell voltage but increases the short-circuit current so that the overall PCE does not change significantly, as evidenced by samples annealed under a range of conditions.

Photogenerated-carrier lifetimes are a major limiting factor of PCE in CZTS^{183–185} and are shorter than in

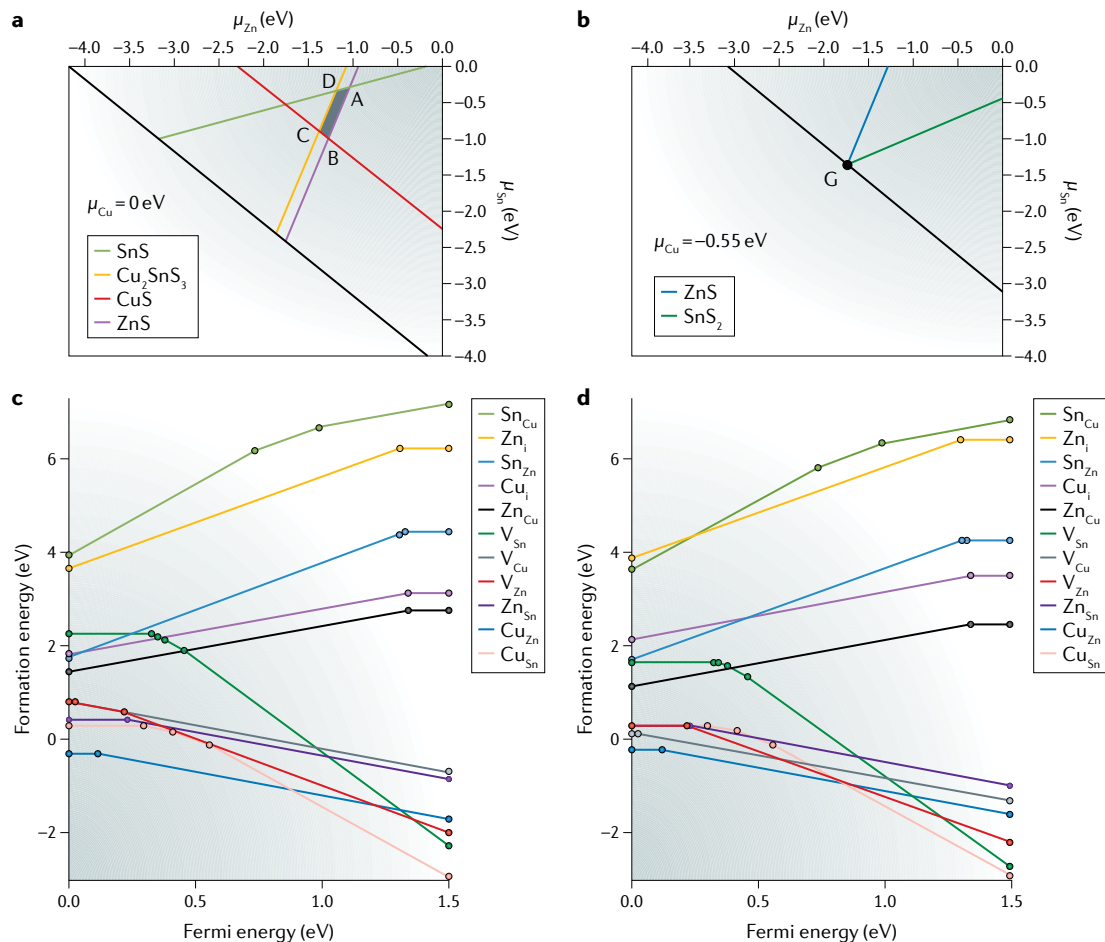


Fig. 3 | Atomic chemical potentials that stabilize the formation of CZTS and the formation energy of point defects under two growth conditions. The stability condition of the quaternary kesterite $\text{Cu}_2\text{ZnSnS}_4$ (CZTS) with respect to its elements ($2\mu_{\text{Cu}} + \mu_{\text{Zn}} + \mu_{\text{Sn}} + 4\mu_{\text{S}} < \Delta H_f$, where μ is the chemical potential and ΔH_f is the enthalpy of formation) is further constrained by the formation of secondary phases. **a** | The stable chemical potential region of CZTS in the $(\mu_{\text{Zn}}, \mu_{\text{Sn}})$ plane with $\mu_{\text{Cu}} = 0 \text{ eV}$. CZTS becomes more stable than its secondary phases in the black shaded area, which is bound by regions in which both CZTS and a secondary phase can form. This numerical analysis reveals the stable conditions for materials synthesis. The reference for each chemical potential (0 eV) is the element in its standard state; for example, the extreme Cu-rich condition was considered by setting the chemical potential of Cu to that of metal Cu ($\mu_{\text{Cu}} = 0 \text{ eV}$). The intersection points of the lines are denoted A–D. **b** | The stable chemical potential region of CZTS in the $(\mu_{\text{Zn}}, \mu_{\text{Sn}})$ plane with $\mu_{\text{Cu}} = -0.55 \text{ eV}$. CZTS can form only at point G because of the low chemical potential of Cu. **c,d** | The plots show the formation energy of native defects in CZTS under conditions C (Cu-rich, panel **c**) and G (Cu-poor, panel **d**). Adapted with permission from REF.¹⁶⁶, American Physical Society.

other technologies (TABLE 1). One of the primary causes is the presence of donor defects that trap minority carriers (electrons). During the deep-level recombination process (BOX 3), the excess energy is dissipated by multiphonon (heat) emission. Recently, the sulfur vacancy was identified as a possible recombination centre in CZTS¹⁸⁶. However, it is yet unclear which defects act as the main non-radiative recombination centres in CZTS or how they can be removed or suppressed. Again, further theoretical and experimental studies are required to shed light on this topic and to increase the performance of kesterite solar cells.

Halide perovskites

Semiconducting metal halides that adopt the perovskite crystal structure have been known since the 1950s¹⁸⁷, and two decades later, the hybrid organic–inorganic halide

perovskite methylammonium lead iodide ($\text{CH}_3\text{NH}_3\text{PbI}_3$) was reported¹⁸⁸. The first photovoltaic devices based on $\text{CH}_3\text{NH}_3\text{PbI}_3$ were in a dye-sensitized solar cell configuration¹⁸⁹, however, these have since been extended to solid-state mesoporous and thin-film architectures with PCEs exceeding 22% in small cells¹⁹⁰. The building blocks of these materials are an anionic framework of corner-sharing lead iodide octahedra (PbI_6^{4-}) with a cation (for example, caesium, methylammonium or formamidinium) present at the centre of each cuboctahedral cage (FIG. 1g). The upper valence band is formed from the antibonding combination of filled Pb 6s and I 5p orbitals, and the lower conduction band is formed from the empty Pb 6p orbitals¹⁹¹ (FIG. 1h). The electron and hole effective masses are light (<0.2 m_e)¹⁹². The high-frequency relative dielectric constant of $\text{CH}_3\text{NH}_3\text{PbI}_3$ is 5, which increases to a static relative dielectric constant of ~24 with the

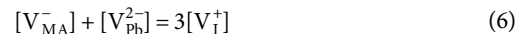
inclusion of lattice vibrations and to a value of ~33 when dipolar molecular rotations are also included¹⁹³.

$\text{CH}_3\text{NH}_3\text{PbI}_3$ and related materials exhibit unusual defect physics. The dominant point defects are site vacancies that have been predicted to have shallow donor and acceptor levels, which are useful for photovoltaic applications¹⁹⁴. Moreover, despite being processed at low temperature from solution, carrier mobilities and lifetimes in perovskites are not severely limited by lattice defects. The defect tolerance of perovskites arises from the low concentrations of deep sub-bandgap levels, which has been understood in terms of the antibonding nature of the electronic band edges, in addition to effective dielectric screening^{195,196}. In the development of perovskite solar cells, little attention has been paid to point defects because high-performance solar cells can be achieved using standard processing routes. However, further improvements in device performance will require careful control of non-radiative processes, which currently limit the open-circuit voltage to 0.1–0.2 V below the radiative limit¹⁹⁷.

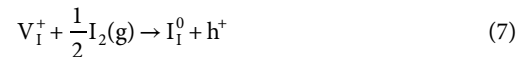
Compared with the other systems discussed above, there is limited information available on point defects in halide perovskites. Moreover, particular care has to be given to the interpretation of temperature-dependent measurements for these materials as they undergo a number of structural phase transitions and the dielectric permittivity exhibits a strong temperature dependence^{193,198}. Recently, the presence of deep-level defects in halide perovskites has been confirmed. In one study, thermally stimulated current measurements were used to probe the defect levels in $\text{CH}_3\text{NH}_3\text{PbI}_3$ solar cells. Four peaks were observed in the thermally stimulated current spectra, two of which were attributed to shallow centres, a third to a phase transition and the fourth to a trap state at ~0.5 eV from a band edge with a density of 10^{15} cm^{-3} (REF. ¹⁹⁹). In a deep-level transient spectroscopy study of high-performance devices based on formamidinium lead halide perovskites, three peaks were reported at 0.82 eV, 0.78 eV and 0.46 eV below the conduction band²⁰⁰. The peaks at 0.82 eV and 0.78 eV were found to have the highest carrier capture cross section but were suppressed when the material was processed in an iodine-rich environment. Despite being a common probe for inorganic semiconductors, results from deep-level spectroscopic studies of hybrid perovskites must be interpreted with caution as perovskites are mixed ionic-electronic conductors with activation energies for ion diffusion that fall in an energy range similar to the measured defect levels¹¹, and ion transport can be enhanced under illumination²⁰¹.

The first-principles calculation of accurate defects levels in Pb-containing perovskites is problematic as a quantitative description of the electronic structure requires a relativistic description, including spin-orbit coupling, which results in a large renormalization of the bandgap^{192,202}. Furthermore, the predicted defect levels have been shown to be sensitive to the choice of electronic structure Hamiltonian²⁰³. There is agreement among calculations that site vacancies involving methylammonium, Pb and I — predicted to be the

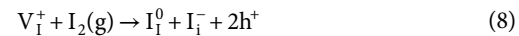
dominant point defects²⁰⁴ — do not result in sub-bandgap levels. Despite the facile ionization of these donor and acceptor defects, the low carrier concentrations ($<10^{15} \text{ cm}^{-3}$) that are commonly observed for the lead halide perovskites can be explained by ionic compensation²⁰⁵. In the Schottky limit, the total concentrations of oppositely charged defects balance as shown in equation 6 (where MA is methylammonium), which decreases the concentrations of free electrons and holes.



The most likely candidate for deep levels is excess iodine in the form of iodine interstitials²⁰⁶, which have been shown to be efficient at trapping holes. These hole-trapping centres are associated with I–I bond formation, which has been well established in other metal halide compounds^{207,208}. Annealing a perovskite film in excess iodine can fill iodine vacancies, resulting in the generation of holes (equation 7).



Additionally, annealing can result in the formation of interstitial defects; for example,



Indeed, treatment using iodine vapour has been found to increase both the electrical conductivity and hole concentration (as the Fermi level can shift more than 100 meV towards the valence band edge)²⁰⁹.

We are far from a clear understanding of defect processes in halide perovskites, in particular those relating to the effect of light on defect formation and transport, which are the subject of ongoing investigations^{210–213}. In Sn-based perovskites, an additional complication is the balance between Sn(II) and Sn(IV), which can result in non-stoichiometry and high levels of electrical conductivity²¹⁴. In double perovskites, in which Pb(II) is replaced by a mixture of valence I and III metals, the high concentration of low-energy antisite defects can give rise to order-disorder behaviour in the cation sublattice²¹⁵. Beyond processes involving native defects, there has been no clear demonstration of an all-perovskite p–n junction, and currently all high-performance Pb perovskite solar cells use an intrinsic (thus, low doping level) perovskite layer in p–i–n-type configurations. The design and demonstration of effective donor and acceptor dopants would allow for new solar cell architectures and application areas to be realized.

Principles for defect control

Each semiconducting material exhibits a distinct defect and doping selectivity, which are dictated by the underlying chemical bonding and crystal structure, and much research effort has been invested into understanding the underlying mechanics¹⁹⁶. In this section, we outline a set of principles concerning defect control in semiconductors for solar cells.

Overcoming doping limits. In photovoltaic devices, it is necessary to control doping levels and carrier concentrations to fabricate effective semiconductor junctions and tune key material parameters, including electrical resistivity, depletion widths and Fermi-level splitting.

Two types of behaviour limit the efficiency of doping: solubility limits, which occur when the equilibrium concentration of a dopant is too low, and charge compensation limits, which arise when the charge of a dopant is cancelled either by a competing configuration (for example, Na_{Cd}^- versus Na_i^+ in CdTe) or other native charged point defects in the system (such as V_{Cu}^- versus $\text{In}_{\text{Cu}}^{2+}$ in CuInS₂). Solubility limits can be influenced by the growth conditions (chemical potentials) and can even be bypassed by using non-equilibrium synthetic procedures²¹⁶. Charge compensation, however, is more restrictive: if the formation energy of a compensating defect becomes negative, it will form spontaneously (so-called charge-killer defects)²¹⁷. The Fermi level (and thus carrier concentrations) in a semiconductor will be pinned at an energy that corresponds to the formation energy of this spontaneous defect, and pinning levels have been observed in many compounds^{205,218}.

One solution to overcome the doping bottlenecks of semiconductors is to tune the processing conditions. For a binary material, AB, formed of a cation A⁺ and anion B⁻, n-type (electron) doping will require the suppression of V_A^- defects and therefore cation-rich growth conditions. Conversely, p-type (hole) doping will require the suppression of V_B^+ defects and therefore anion-rich growth conditions^{219,220}. In the context of halide perovskites, p-type doping could be achieved by replacing some lattice Pb²⁺ by Ag⁺, forming Ag_{Pb}^- ; however, it would be necessary to prevent the formation of compensating I vacancies. Although hole compensation is desired — that is, $[\text{Ag}_{\text{Pb}}^-] = [\text{h}^+]$ — the spontaneous loss of I is likely to result in $[\text{Ag}_{\text{Pb}}^-] = [\text{V}_I^+]$, which negates the effect of acceptor doping. One approach is to simultaneously introduce a dopant while controlling the chemical potential of I, for example, by processing the acceptor-doped material in an I-rich atmosphere. In this way, it may be possible to develop robust p-type and n-type halide perovskites.

A second solution for increasing doping efficiency is to choose an alternative host compound with a more favourable electronic structure. It has been observed that p-type doping is favoured in materials with ‘high’ valence bands close to the vacuum level, whereas n-type doping is favoured in materials with ‘low’ conduction bands²²¹. This behaviour can be understood simply by considering that a low ionization potential facilitates hole formation and a high electron affinity stabilizes excess electrons²²². The band energies of a semiconductor can be controlled either by manipulating the chemistry (through compositional engineering) or structure (through crystal engineering). For example, a valence band that is more amenable to p-type doping can be achieved by incorporating ions with low-binding-energy valence orbitals, such as Cu⁺ 3d¹⁰, Ag⁺ 4d¹⁰, Sn²⁺ 5s² and Pb²⁺ 6s², whereas it has been shown that the valence band of TiO₂ can be modified by several eV simply by changing the polymorph (for example, from rutile to anatase or brookite)²²³.

Enhancing carrier lifetime. The lifetime of charge carriers in solar cells can be as essential for achieving high performance as the doping density. The development of Si technology has shown the importance of controlling intrinsic defects and dopants¹⁷, unintentional extrinsic impurities²⁹ and defects formed under operating conditions^{57,64} to achieve high light-to-electricity conversion efficiency.

Carrier lifetimes are reduced by trapping in deep defect centres and ultimately through recombination between electrons and holes. Solar cells usually operate in a low carrier density regime ($n < 10^{17} \text{ cm}^{-3}$, where n is the concentration of photogenerated charge carriers) in which monomolecular recombination dominates; therefore, careful control of the concentration of deep-level defects is essential (BOX 3). The physical process of non-radiative defect-assisted recombination is complex and couples the electronic and vibrational states of a material, and thus, there are few established guidelines. In Si, chemical passivation is used to remove dangling bonds, whereas in CIGS, defect–defect interactions that form charge-neutral clusters serve to remove deep electron and hole traps. Over the past 5 years, there has been significant progress in the first-principles description of the capture cross section and recombination rates for point defects in semiconductors^{186,224,225}, which may enable the development of new structure–property maps, as well as design procedures and principles, in the near future.

Practically, photogenerated-carrier lifetimes are enhanced not only by the removal of defects and impurities but also through changes in the device architecture. Several approaches have been pioneered in Si technologies, such as spatial modulation of the Fermi level with back-surface fields²²⁶ and heavily doped regions near the electrical contacts¹⁵, in order to reduce the spatial overlap between the defects and charge carriers.

Other solar cell technologies share the same fundamental working principles as Si and thus the above concepts can be adapted to enhance performance. For example, the concept of the spatial separation of charge carriers and recombination sites has been realized in CIGS²²⁷ using a gradient in the In:Ga composition ratio, which raises the conduction band of the absorber material near the contacts and reduces interfacial recombination rates. More recently, First Solar developed bandgap-graded CdTe solar cells²²⁸ using a Cd(Se,Te) absorber layer. The spatial separation approach could be adapted for CZTS, for example, through the use of (Ag,Cu), (Zn,Cd) or (S,Se) chemical gradients. Halide perovskites and newly emerging systems, such as SnS, CuSbS₃ and FeS₂, may also benefit from these advances to overcome their high recombination rates and low cell voltages. For example, SnS has a bandgap of 1.1 eV, which makes it comparable to Si, yet the highest recorded PCE of a SnS solar cell is below 5%, and the open-circuit voltage is only 0.4 V (REF.²²⁹). The minority-carrier lifetime of SnS has been recently improved from <1 ns to >3 ns by avoiding low concentrations of extrinsic impurities²³⁰; this approach has not solved the carrier lifetime problem but illustrates the importance of defect engineering.

Overall, we can distil the above principles for defect engineering down to two main objectives: first,

overcoming doping bottlenecks for the optimization of electron (donor) and hole (acceptor) concentrations by changing the growth conditions or by chemical modification of the host material, and second, enhancing the lifetime of charge carriers by identifying deep-level, killer defects that may be present at very low concentrations and devising strategies to deactivate or remove them.

Outlook

In the search for new photovoltaic materials, the magnitude of the bandgap and visible-range absorption spectrum are useful selection metrics^{231–233}. We argue that consideration of point defect processes is just as essential. Although a material may absorb sunlight, the presence of detrimental defects can severely hinder its ability to generate and transport photogenerated charge carriers. There is an abundance of materials with bandgaps in the visible range (1–3 eV), which make them attractive from consideration of the theoretical Shockley–Queisser limit, but very few classes of semiconductors have resulted in photovoltaic efficiencies above 10%. This is due to both the inability to control the equilibrium concentrations of electrons and holes (that is, limits to doping) and the presence of efficient non-radiative pathways that often

involve sub-bandgap electronic states introduced by intrinsic defects and extrinsic impurities (resulting in low carrier lifetimes).

The defect physics and chemistry of novel materials should be carefully assessed to screen and predict plausible high-efficiency photovoltaic materials. Indeed, defect tolerance has been proposed as a guiding principle for discovering new compounds^{195,234–237}. However, the wide range of defect levels and processes found in current technologies (TABLE 2) reflects that the majority of known semiconductors are not naturally defect tolerant. Instead, processing routes and chemical treatments have been carefully developed over time to minimize the effects of the most detrimental species. We recognize that point defects are much harder to screen, measure and predict than bandgaps; however, we suggest that a greater consideration of defects with close collaboration between theoretical and experimental investigators, and between academic and industrial researchers, is required to develop more realistic and robust design procedures for next-generation solar energy solutions.

Published online 22 June 2018

1. Pantelides, S. T. The electronic structure of impurities and other point defects in semiconductors. *Rev. Mod. Phys.* **50**, 797–858 (1978).
2. Stoneham, A. M. *Theory of Defects in Solids* (Oxford Univ. Press, 1975).
3. Frenkel, J. Über die Wärmebewegung in festen und flüssigen Körpern [German]. *Z. Physik.* **35**, 652–669 (1926).
4. Kroger, F. A. & Vink, H. J. Relations between the concentrations of imperfections in solids. *J. Phys. Chem. Solids* **5**, 208–223 (1958).
5. Mott, N. F. & Littleton, M. J. Conduction in polar crystals. I. Electrolytic conduction in solid salts. *Trans. Faraday Soc.* **34**, 485–499 (1938).
6. Freysoldt, C. et al. First-principles calculations for point defects in solids. *Rev. Mod. Phys.* **86**, 253–305 (2014).
7. Bracht, H., Haller, E. E. & Clark-Phelps, R. Silicon self-diffusion in isotope heterostructures. *Phys. Rev. Lett.* **81**, 393–396 (1998).
8. Jones, E. D., Stewart, N. M. & Mullin, J. B. Studies on the self-diffusion of cadmium in cadmium telluride in the temperature range 350–650 °C using anodic oxidation. *J. Cryst. Growth* **130**, 6–12 (1993).
9. Gartsman, K. et al. Direct evidence for diffusion and electromigration of Cu in CuInSe₂. *J. Appl. Phys.* **82**, 4282–4285 (1997).
10. Istratov, A. A., Flink, C., Hieslmair, H., Weber, E. R. & Heiser, T. Intrinsic diffusion coefficient of interstitial copper in silicon. *Phys. Rev. Lett.* **81**, 1243–1246 (1998).
11. Eames, C. et al. Ionic transport in hybrid lead iodide perovskite solar cells. *Nat. Commun.* **6**, 7497 (2015).
12. Buckridge, J. et al. Determination of the nitrogen vacancy as a shallow compensating center in GaN doped with divalent metals. *Phys. Rev. Lett.* **114**, 016405 (2015).
13. Madelung, O. M. *Semiconductors: Data Handbook* (Springer, 2003).
14. De Wolf, S., Descoedres, A., Holman, Z. C. & Ballif, C. High-efficiency silicon heterojunction solar cells: a review. *Green* **2**, 7–24 (2012).
15. Battaglia, C., Cuevas, A. & De Wolf, S. High-efficiency crystalline silicon solar cells: status and perspectives. *Energy Environ. Sci.* **9**, 1552–1576 (2016).
16. Newman, R. C. Defects in silicon. *Rep. Prog. Phys.* **45**, 1163–1210 (1982).
17. Fahey, P. M., Griffin, P. B. & Plummer, J. D. Point defects and dopant diffusion in silicon. *Rev. Mod. Phys.* **61**, 289–384 (1989).
18. Adachi, D., Hernández, J. L. & Yamamoto, K. Impact of carrier recombination on fill factor for large area heterojunction crystalline silicon solar cell with 25.1% efficiency. *Appl. Phys. Lett.* **107**, 233506 (2015).
19. Pankove, J. I. & Tarn, M. L. Amorphous silicon as a passivant for crystalline silicon. *Appl. Phys. Lett.* **34**, 156–157 (1979).
20. Aberle, A. G. Surface passivation of crystalline silicon solar cells: a review. *Prog. Photovolt.* **8**, 473–487 (2000).
21. Richter, A., Hermle, M. & Glunz, S. W. Crystalline silicon solar cells reassessment of the limiting efficiency for crystalline silicon solar cells. *IEEE J. Photovolt.* **3**, 1184–1191 (2013).
22. Broqvist, P., Alkauskas, A. & Pasquarello, A. Defect levels of dangling bonds in silicon and germanium through hybrid functionals. *Phys. Rev. B* **78**, 075203 (2008).
23. George, B. M. et al. Atomic structure of interface states in silicon heterojunction solar cells. *Phys. Rev. Lett.* **110**, 1–5 (2013).
24. Higashi, G. S., Chabal, Y. J., Trucks, G. W. & Raghavachari, K. Ideal hydrogen termination of the Si(111) surface. *Appl. Phys. Lett.* **56**, 656–658 (1990).
25. Chang, K. J. & Chadi, D. J. Hydrogen bonding and diffusion in crystalline silicon. *Phys. Rev. B* **40**, 11644–11653 (1989).
26. Hoex, B., Gielis, J. J. H., van de Sanden, M. C. M. & Kessels, W. M. M. On the c-Si surface passivation mechanism by the negative-charge-dielectric Al₂O₃. *J. Appl. Phys.* **104**, 113703 (2008).
27. Davis, J. R. et al. Impurities in silicon solar cells. *IEEE Trans. Electron. Devices* **27**, 677–687 (1980).
28. Coletti, G. et al. Impact of metal contamination in silicon solar cells. *Adv. Funct. Mater.* **21**, 879–890 (2011).
29. Peaker, A. R. et al. Recombination via point defects and their complexes in solar silicon. *Phys. Status Solidi A* **209**, 1884–1893 (2012).
30. Gilles, D., Schröter, W. & Bergholz, W. Impact of the electronic structure on the solubility and diffusion of 3d transition elements in silicon. *Phys. Rev. B* **41**, 5770–5782 (1990).
31. Zimmermann, H. & Ryssel, H. Gold and platinum diffusion: the key to the understanding of intrinsic point-defect behavior in silicon. *Appl. Phys. A* **55**, 121–134 (1992).
32. Lemke, H. Properties of silicon crystals doped with zirconium or hafnium. *Phys. Status Solidi A* **122**, 617–630 (1990).
33. Istratov, A. A., Buonassisi, T., Pickett, M. D., Heuer, M. & Weber, E. R. Control of metal impurities in 'dirty' multicrystalline silicon for solar cells. *Mater. Sci. Eng. B* **134**, 282–286 (2006).
34. Hofstetter, J., Lelièvre, J. F., del Cañizo, C. & Luque, A. Acceptable contamination levels in solar grade silicon: from feedstock to solar cell. *Mater. Sci. Eng. B* **159–160**, 299–304 (2009).
35. Pizzini, S. Towards solar grade silicon: challenges and benefits for low cost photovoltaics. *Sol. Energy Mater. Sol. Cells* **94**, 1528–1533 (2010).
36. Reinders, A., Verlinden, P., van Sark, W. & Freundlich, A. *Photovoltaic Solar Energy: From Fundamentals to Applications* (Wiley, 2017).
37. Weber, E. R. Transition metals in silicon. *Appl. Phys. A* **30**, 1–22 (1983).
38. Myers, S. M., Seibt, M. & Schröter, W. Mechanisms of transition-metal gettering in silicon. *J. Appl. Phys.* **88**, 3795 (2000).
39. Rein, S. & Glunz, S. W. Electronic properties of interstitial iron and iron-boron pairs determined by means of advanced lifetime spectroscopy. *J. Appl. Phys.* **98**, 113711 (2005).
40. Istratov, A. A. et al. Nickel solubility in intrinsic and doped silicon. *J. Appl. Phys.* **97**, 023505 (2005).
41. Diez, S., Rein, S., Roth, T. & Glunz, S. W. Cobalt related defect levels in silicon analyzed by temperature- and injection-dependent lifetime spectroscopy. *J. Appl. Phys.* **101**, 033710 (2007).
42. Steger, M. et al. Photoluminescence of deep defects involving transition metals in Si: new insights from highly enriched ²⁸Si. *J. Appl. Phys.* **110**, 081301 (2011).
43. Markevich, V. P. et al. Titanium in silicon: lattice positions and electronic properties. *Appl. Phys. Lett.* **104**, 152105 (2014).
44. Marinopoulos, A. G., Santos, P. & Coutinho, J. DFT+U study of electrical levels and migration barriers of early 3d and 4d transition metals in silicon. *Phys. Rev. B* **92**, 075124 (2015).
45. Sharan, A., Gui, Z. & Janotti, A. Hybrid-functional calculations of the copper impurity in silicon. *Phys. Rev. Appl.* **8**, 024023 (2017).
46. Buonassisi, T. et al. Engineering metal-impurity nanodefects for low-cost solar cells. *Nat. Mater.* **4**, 676–679 (2005).
47. Pickett, M. D. & Buonassisi, T. Iron point defect reduction in multicrystalline silicon solar cells. *Appl. Phys. Lett.* **92**, 2006–2009 (2008).
48. Alkauskas, A., McCluskey, M. D. & Van de Walle, C. G. Tutorial: defects in semiconductors — combining experiment and theory. *J. Appl. Phys.* **119**, 181101 (2016).
49. Watkins, G. D. Native defects and their interactions with impurities in silicon. *MRS Proc.* **469**, 139 (1997).
50. Tuomisto, F. & Makkonen, I. Defect identification in semiconductors with positron annihilation: experiment and theory. *Rev. Mod. Phys.* **85**, 1583–1631 (2013).
51. Stavola, M. & Fowler, W. B. Tutorial: novel properties of defects in semiconductors revealed by their vibrational spectra. *J. Appl. Phys.* **123**, 161561 (2018).

52. McPhail, D. S. Applications of secondary ion mass spectrometry (SIMS) in materials science. *J. Mater. Sci.* **41**, 873–903 (2006).
53. Lindroos, J. et al. Nickel: a very fast diffuser in silicon. *J. Appl. Phys.* **113**, 204906 (2013).
54. Rinke, P., Janotti, A., Scheffler, M. & Van de Walle, C. Defect formation energies without the band-gap problem: combining density-functional theory and the GW approach for the silicon self-interstitial. *Phys. Rev. Lett.* **102**, 026402 (2009).
55. Esterreicher, S. K., Backlund, D. J., Carbone, C. & Scheffler, M. Activation energies for diffusion of defects in silicon: the role of the exchange-correlation functional. *Angew. Chem. Int. Ed.* **50**, 10221–10225 (2011).
56. Spiewak, P. & Kurzydowski, K. J. Formation and migration energies of the vacancy in Si calculated using the HSE06 range-separated hybrid functional. *Phys. Rev. B* **88**, 195204 (2013).
57. Lindroos, J. & Savin, H. Review of light-induced degradation in crystalline silicon solar cells. *Sol. Energy Mater. Sol. Cells* **147**, 115–126 (2016).
58. Nieuwelt, T., Schon, J., Warta, W., Glunz, S. W. & Schubert, M. C. Degradation of crystalline silicon due to boron–oxygen defects. *IEEE J. Photovolt.* **7**, 383–398 (2017).
59. Hallam, B. et al. Recent insights into boron–oxygen related degradation: evidence of a single defect. *Sol. Energy Mater. Sol. Cells* **173**, 25–32 (2017).
60. Taguchi, M. et al. 24.7% Record efficiency HIT solar cell on thin silicon wafer. *IEEE J. Photovolt.* **4**, 96–99 (2014).
61. Masuko, K. et al. Achievement of more than 25% conversion efficiency with crystalline silicon heterojunction solar cell. *IEEE J. Photovolt.* **4**, 1433–1435 (2014).
62. Yoshikawa, K. et al. Silicon heterojunction solar cell with interdigitated back contacts for a photoconversion efficiency over 26%. *Nat. Energy* **2**, 17032 (2017).
63. Bouffard, Y. et al. Experimental evidence on removing copper and light-induced degradation from silicon by negative charge. *Appl. Phys. Lett.* **105**, 182108 (2014).
64. Luo, W. et al. Potential-induced degradation in photovoltaic modules: a critical review. *Energy Environ. Sci.* **10**, 43–68 (2017).
65. Loeferski, J. J. Theoretical considerations governing the choice of the optimum semiconductor for photovoltaic solar energy conversion. *J. Appl. Phys.* **27**, 777–784 (1956).
66. McCandless, B. E. & Sites, J. R. in *Handbook of Photovoltaic Science and Engineering* (eds Luque, A. & Hegedus, S.) 600–641 (John Wiley & Sons, 2011).
67. Green, M. A. et al. Solar cell efficiency tables (version 51). *Prog. Photovolt.* **26**, 2–12 (2018).
68. Wei, S.-H., Zhang, S. B. & Zunger, A. First-principles calculation of band offsets, optical bowings, and defects in CdS, CdSe, CdTe, and their alloys. *J. Appl. Phys.* **87**, 1304–1311 (2000).
69. Ma, J. et al. Dependence of the minority-carrier lifetime on the stoichiometry of CdTe using time-resolved photoluminescence and first-principles calculations. *Phys. Rev. Lett.* **111**, 067402 (2013).
70. Kranz, L. et al. Doping of polycrystalline CdTe for high-efficiency solar cells on flexible metal foil. *Nat. Commun.* **4**, 3306 (2013).
71. Gessert, T. A. et al. Research strategies toward improving thin-film CdTe photovoltaic devices beyond 20% conversion efficiency. *Sol. Energy Mater. Sol. Cells* **119**, 149–155 (2013).
72. Reese, M. O. et al. Intrinsic surface passivation of CdTe. *J. Appl. Phys.* **118**, 155305 (2015).
73. Burst, J. M. et al. CdTe solar cells with open-circuit voltage breaking the 1 V barrier. *Nat. Energy* **1**, 16015 (2016).
74. Kanevce, A., Reese, M. O., Barnes, T. M., Jensen, S. A. & Metzger, W. K. The roles of carrier concentration and interface, bulk, and grain-boundary recombination for 25% efficient CdTe solar cells. *J. Appl. Phys.* **121**, 214506 (2017).
75. Yang, J.-H., Yin, W.-J., Park, J.-S., Ma, J. & Wei, S.-H. Review on first-principles study of defect properties of CdTe as a solar cell absorber. *Semicond. Sci. Technol.* **31**, 083002 (2016).
76. Shepidchenko, A., Sanyal, B., Klintenberg, M. & Mirbt, S. Small hole polaron in CdTe: Cd-vacancy revisited. *Sci. Rep.* **5**, 14509 (2015).
77. Lindström, A., Mirbt, S., Sanyal, B. & Klintenberg, M. High resistivity in undoped CdTe: carrier compensation of Te antisites and Cd vacancies. *J. Phys. D* **49**, 035101 (2016).
78. Yang, J. H., Yin, W. J., Park, J. S., Metzger, W. & Wei, S. H. First-principles study of roles of Cu and Cl in polycrystalline CdTe. *J. Appl. Phys.* **119**, 045104 (2016).
79. Yang, J. H. et al. Tuning the Fermi level beyond the equilibrium doping limit through quenching: the case of CdTe. *Phys. Rev. B* **90**, 245202 (2014).
80. Pautrat, J. L., Francou, J. M., Magnea, N., Molva, E. & Saminadayar, K. Donors and acceptors in tellurium compounds: the problem of doping and self-compensation. *J. Cryst. Growth* **72**, 194–204 (1985).
81. Said, M. & Kanehisa, M. A. Excited states of acceptors in CdTe and ZnTe. *J. Cryst. Growth* **101**, 488–492 (1990).
82. Poplawsky, J. D. et al. Direct imaging of Cl- and Cu-induced short-circuit efficiency changes in CdTe solar cells. *Adv. Energy Mater.* **4**, 1400454 (2014).
83. Kuciauskas, D. et al. The impact of Cu on recombination in high voltage CdTe solar cells. *Appl. Phys. Lett.* **107**, 243906 (2015).
84. Kuciauskas, D. et al. Recombination analysis in cadmium telluride photovoltaic solar cells with photoluminescence spectroscopy. *IEEE J. Photovolt.* **6**, 313–318 (2016).
85. Yang, J. H., Metzger, W. K. & Wei, S. H. Carrier providers or killers: the case of Cu defects in CdTe. *Appl. Phys. Lett.* **111**, 042106 (2017).
86. Yang, J.-H., Park, J.-S., Kang, J. & Wei, S.-H. First-principles multiple-barrier diffusion theory: the case study of interstitial diffusion in CdTe. *Phys. Rev. B* **91**, 075202 (2015).
87. Yang, J. H. et al. Enhanced p-type dopability of P and As in CdTe using non-equilibrium thermal processing. *J. Appl. Phys.* **118**, 025102 (2015).
88. Mooney, P. M. Deep donor levels (DX centers) in III–V semiconductors. *J. Appl. Phys.* **67**, R1–R26 (1990).
89. Wei, S.-H. & Zhang, S. B. Chemical trends of defect formation and doping limit in II–VI semiconductors: the case of CdTe. *Phys. Rev. B* **66**, 155211 (2002).
90. Barnard, E. S. et al. 3D Lifetime tomography reveals how CdCl₂ improves recombination throughout CdTe solar cells. *Adv. Mater.* **29**, 1603801 (2017).
91. Moravec, P., Hage-Ali, M., Chibani, L. & Siffert, P. Deep levels in semi-insulating CdTe. *Mater. Sci. Eng. B* **16**, 223–227 (1993).
92. Balcioglu, A., Ahrenkiel, R. K. & Hasoon, F. Deep-level impurities in CdTe/CdS thin-film solar cells. *J. Appl. Phys.* **88**, 7175–7178 (2000).
93. Mathew, X. Photo-induced current transient spectroscopic study of the traps in CdTe. *Sol. Energy Mater. Sol. Cells* **76**, 225–242 (2003).
94. Komin, V. et al. The effect of the CdCl₂ treatment on CdTe/CdS thin film solar cells studied using deep level transient spectroscopy. *Thin Solid Films* **431**, 143–147 (2003).
95. Elhadidy, H., Franc, J., Moravec, P., Höschl, P. & Fiederle, M. Deep level defects in CdTe materials studied by thermoelectric effect spectroscopy and photoinduced current transient spectroscopy. *Semicond. Sci. Technol.* **22**, 537–542 (2007).
96. Castaldini, A., Cavallini, A., Fraboni, B., Fernandez, P. & Piqueras, J. Deep energy levels in CdTe and CdZnTe. *J. Appl. Phys.* **83**, 2121–2126 (1998).
97. Kuciauskas, D. et al. Charge-carrier transport and recombination in heteroepitaxial CdTe. *J. Appl. Phys.* **116**, 123108 (2014).
98. Li, C. et al. From atomic structure to photovoltaic properties in CdTe solar cells. *Ultramicroscopy* **134**, 113–125 (2013).
99. Li, C. et al. Grain-boundary-enhanced carrier collection in CdTe solar cells. *Phys. Rev. Lett.* **112**, 156103 (2014).
100. Park, J.-S., Yang, J.-H., Barnes, T. & Wei, S.-H. Effect of intermixing at CdS/CdTe interface on defect properties. *Appl. Phys. Lett.* **109**, 14–18 (2016).
101. Moseley, J. et al. Recombination by grain-boundary type in CdTe. *J. Appl. Phys.* **118**, 025702 (2015).
102. Visoly-Fisher, I., Cohen, S. R., Ruzin, A. & Cahen, D. How polycrystalline devices can outperform single-crystal ones: thin film CdTe/CdS solar cells. *Adv. Mater.* **16**, 879–883 (2004).
103. Visoly-Fisher, I., Cohen, S. R., Gartsman, K., Ruzin, A. & Cahen, D. Understanding the beneficial role of grain boundaries in polycrystalline solar cells from single-grain-boundary scanning probe microscopy. *Adv. Funct. Mater.* **16**, 649–660 (2006).
104. Major, J. D. Grain boundaries in CdTe thin film solar cells: a review. *Semicond. Sci. Technol.* **31**, 093001 (2016).
105. Yan, Y., Al-Jassim, M. M. & Jones, K. M. Structure and effects of double-positioning twin boundaries in CdTe. *J. Appl. Phys.* **94**, 2976–2979 (2003).
106. Zhang, L. et al. Effect of copassivation of Cl and Cu on CdTe grain boundaries. *Phys. Rev. Lett.* **101**, 155501 (2008).
107. Yang, J.-H., Shi, L., Wang, L.-W. & Wei, S.-H. Non-radiative carrier recombination enhanced by two-level process: a first-principles study. *Sci. Rep.* **6**, 21712 (2016).
108. Durose, K., Edwards, P. R. & Halliday, D. P. Materials aspects of CdTe/CdS solar cells. *J. Cryst. Growth* **197**, 733–742 (1999).
109. Dharmadasa, I. Review of the CdCl₂ treatment used in CdS/CdTe thin film solar cell development and new evidence towards improved understanding. *Coatings* **4**, 282–307 (2014).
110. Yoo, S. et al. Identification of critical stacking faults in thin-film CdTe solar cells. *Appl. Phys. Lett.* **105**, 062104 (2014).
111. Kranz, L. et al. Tailoring impurity distribution in polycrystalline CdTe solar cells for enhanced minority carrier lifetime. *Adv. Energy Mater.* **4**, 1301400 (2014).
112. Jensen, S. A. et al. Long carrier lifetimes in large-grain polycrystalline CdTe without CdCl₂. *Appl. Phys. Lett.* **108**, 263903 (2016).
113. Ringel, S. A., Smith, A. W., MacDougal, M. H. & Rohatgi, A. The effects of CdCl₂ on the electronic properties of molecular-beam epitaxially grown CdTe/CdS heterojunction solar cells. *J. Appl. Phys.* **70**, 881–889 (1991).
114. Moutinho, H. R., Al-Jassim, M. M., Levi, D. H., Dippo, P. C. & Kazmerski, L. L. Effects of CdCl₂ treatment on the recrystallization and electro-optical properties of CdTe thin films. *J. Vac. Sci. Technol. A* **16**, 1251–1257 (1998).
115. Abbas, A. et al. The effect of cadmium chloride treatment on close-spaced sublimated cadmium telluride thin-film solar cells. *IEEE J. Photovolt.* **3**, 1361–1366 (2013).
116. McCandless, B. E., Moulton, L. V. & Birkmire, R. W. Recrystallization and sulfur diffusion in CdCl₂-treated CdTe/CdS thin films. *Prog. Photovolt.* **5**, 249–260 (1997).
117. Metzger, W. K., Albin, D., Romero, M. J., Dippo, P. & Young, M. CdCl₂ treatment, S diffusion, and recombination in polycrystalline CdTe. *J. Appl. Phys.* **99**, 103703 (2006).
118. Williams, B. L. et al. A comparative study of the effects of nontoxic chloride treatments on CdTe solar cell microstructure and stoichiometry. *Adv. Energy Mater.* **5**, 1500554 (2015).
119. Major, J. D., Treherne, R. E., Phillips, L. J. & Durose, K. A low-cost non-toxic post-growth activation step for CdTe solar cells. *Nature* **511**, 334–337 (2014).
120. Jaffe, J. E. & Zunger, A. Electronic structure of the ternary chalcopryite semiconductors CuAlS₂, CuGaS₂, CuInS₂, CuAlSe₂, CuGaSe₂, and CuInSe₂. *Phys. Rev. B* **28**, 5822–5847 (1983).
121. Butler, D. Thin films: ready for their close-up? *Nature* **454**, 558–559 (2008).
122. Noufi, R., Axton, R., Herrington, C. & Deb, S. K. Electronic properties versus composition of thin films of CuInSe₂. *Appl. Phys. Lett.* **45**, 668–670 (1984).
123. Wei, S.-H., Zhang, S. B. & Zunger, A. Effects of Ga addition to CuInSe₂ on its electronic, structural, and defect properties. *Appl. Phys. Lett.* **72**, 3199–3201 (1998).
124. Zhang, S. B., Wei, S.-H., Zunger, A. & Katayama-Yoshida, H. Defect physics of the CuInSe₂ chalcopryite semiconductor. *Phys. Rev. B* **57**, 9642–9656 (1998).
125. Stephan, C., Schorr, S., Tovar, M. & Schock, H.-W. Comprehensive insights into point defect and defect cluster formation in CuInSe₂. *Appl. Phys. Lett.* **98**, 091906 (2011).
126. Malitkaya, M., Komasa, H. P., Havu, V. & Puska, M. J. First-principles modeling of point defects and complexes in thin-film solar-cell absorber CuInSe₂. *Adv. Electron. Mater.* **3**, 1600353 (2017).
127. Pohl, J. & Albe, K. Intrinsic point defects in CuInSe₂ and CuGaSe₂ as seen via screened-exchange hybrid density functional theory. *Phys. Rev. B* **87**, 245203 (2013).
128. Fearhiley, M. L. The phase relations in the Cu, In, Se system and the growth of CuInSe₂ single crystals. *Sol. Cells* **16**, 91–100 (1986).
129. Han, S.-H., Hasoon, F. S., Al-Thani, H. A., Hermann, A. M. & Levi, D. H. Effect of Cu deficiency on the defect levels of Cu_{0.86}In_{1.05}Se_{2.05} determined by spectroscopic ellipsometry. *Appl. Phys. Lett.* **86**, 021903 (2005).
130. Schmid, D., Ruckh, M., Grunwald, F. & Schock, H. W. Chalcopryrite/defect chalcopryite heterojunctions on the basis of CuInSe₂. *J. Appl. Phys.* **73**, 2902–2909 (1993).

131. Ruberto, M. N. & Rothwarf, A. Time-dependent open-circuit voltage in CuInSe_x/CdS solar cells: theory and experiment. *J. Appl. Phys.* **61**, 4662–4669 (1987).
132. Rau, U., Schmitt, M., Parisi, J., Riedl, W. & Karg, F. Persistent photoconductivity in Cu(In, Ga)Se₂ heterojunctions and thin films prepared by sequential deposition. *Appl. Phys. Lett.* **73**, 223–225 (1998).
133. Heath, J. T., Cohen, J. D. & Shafarman, W. N. Bulk and metastable defects in CuIn_{1-x}Ga_xSe₂ thin films using drive-level capacitance profiling. *J. Appl. Phys.* **95**, 1000–1010 (2004).
134. Harvey, S. P., Johnston, S. & Teeter, G. Effects of voltage-bias annealing on metastable defect populations in CIGS and CZTSe solar cells. *2016 IEEE 43rd Photovoltaic Specialists Conference (PVSC)* <https://doi.org/10.1109/PVSC.2016.7750018> (2016).
135. Teeter, G., Harvey, S. P. & Johnston, S. Controlling metastable native point-defect populations in Cu(In, Ga)Se₂ and Cu₂ZnSnSe₄ materials and solar cells through voltage-bias annealing. *J. Appl. Phys.* **121**, 043102 (2017).
136. Zabierski, P., Rau, U. & Igalsen, M. Classification of metastabilities in the electrical characteristics of ZnO/CdS/Cu(In, Ga)Se₂ solar cells. *Thin Solid Films* **387**, 147–150 (2001).
137. Lany, S. & Zunger, A. Light- and bias-induced metastabilities in Cu(In, Ga)Se₂ based solar cells caused by the (V_{Se} – V_{Cu}) vacancy complex. *J. Appl. Phys.* **100**, 113715–113725 (2006).
138. Lang, D. V. & Logan, R. A. Large-lattice-relaxation model for persistent photoconductivity in compound semiconductors. *Phys. Rev. Lett.* **39**, 635–639 (1977).
139. Chadi, D. J. & Chang, K. J. Theory of the atomic and electronic structure of DX centers in GaAs and Al_{1-x}As alloys. *Phys. Rev. Lett.* **61**, 873–876 (1988).
140. Thio, T., Bennett, J. W., Chadi, D. J., Linke, R. A. & Tamargo, M. C. DX centers in II-VI semiconductors and heterojunctions. *J. Electron. Mater.* **25**, 229–233 (1996).
141. Lany, S. & Zunger, A. Intrinsic DX centers in ternary chalcopyrite semiconductors. *Phys. Rev. Lett.* **100**, 016401 (2008).
142. Niles, D. W. et al. Na impurity chemistry in photovoltaic CIGS thin films: investigation with x-ray photoelectron spectroscopy. *J. Vac. Sci. Technol.* **15**, 3044–3049 (1997).
143. Kimura, R. et al. Effects of sodium on CuIn_{1-x}Se_x thin films. *Jpn. J. Appl. Phys.* **38**, L899–L901 (1999).
144. Pianezzi, F. et al. Unveiling the effects of post-deposition treatment with different alkaline elements on the electronic properties of CIGS thin film solar cells. *Phys. Chem. Chem. Phys.* **16**, 8843–8851 (2014).
145. Lammer, M., Klemm, U. & Powalla, M. Sodium co-evaporation for low temperature Cu(In, Ga)Se₂ deposition. *Thin Solid Films* **387**, 33–36 (2001).
146. Wei, S.-H., Zhang, S. B. & Zunger, A. Effects of Na on the electrical and structural properties of CuInSe₂. *J. Appl. Phys.* **85**, 7214–7218 (1999).
147. Oikonen, L. E., Carenchukova, M. G., Seitsonen, A. P. & Nieminen, R. M. Effect of sodium incorporation into CuInSe₂ from first principles. *J. Appl. Phys.* **114**, 083503 (2013).
148. Yuan, Z. K. et al. Na-diffusion enhanced p-type conductivity in Cu(In, Ga)Se₂: a new mechanism for efficient doping in semiconductors. *Adv. Energy Mater.* **6**, 1–7 (2016).
149. Forest, R. V., Eser, E., McCandless, B. E., Chen, J. G. & Birkmire, R. W. Reversibility of (Ag, Cu)(In, Ga)Se₂ electrical properties with the addition and removal of Na: role of grain boundaries. *J. Appl. Phys.* **117**, 115102 (2015).
150. Kronik, L., Cahen, D. & Schock, H. W. Effects of sodium on polycrystalline CuIn_{1-x}Gal_xSe₂ and its solar cell performance. *Adv. Mater.* **10**, 31–36 (1998).
151. Persson, C. & Zunger, A. Anomalous grain boundary physics in polycrystalline CuInSe₂: the existence of a hole barrier. *Phys. Rev. Lett.* **91**, 266401 (2003).
152. Siebenritt, S., Igalsen, M., Persson, C. & Lany, S. The electronic structure of chalcopyrites – bands, point defects and grain boundaries. *Prog. Photovolt.* **18**, 390–410 (2010).
153. Abou-Ras, D. et al. Direct insight into grain boundary reconstruction in polycrystalline Cu(In, Ga)Se₂ with atomic resolution. *Phys. Rev. Lett.* **108**, 075502 (2012).
154. Yin, W.-J., Wu, Y., Noufi, R., Al-Jassim, M. & Yan, Y. Defect segregation at grain boundary and its impact on photovoltaic performance of CuInSe₂. *Appl. Phys. Lett.* **102**, 193905 (2013).
155. Keller, D. et al. Band gap widening at random CIGS grain boundary detected by valence electron energy loss spectroscopy. *Appl. Phys. Lett.* **109**, 153103 (2016).
156. Goodman, C. H. L. The prediction of semiconducting properties in inorganic compounds. *J. Phys. Chem. Solids* **6**, 305–314 (1958).
157. Pamplin, B. R. A systematic method of deriving new semiconducting compounds by structural analogy. *J. Phys. Chem. Solids* **25**, 675–684 (1964).
158. Pamplin, B. R. & Shah, J. S. Studies in the adamantine family of semiconductors. *J. Electrochem. Soc.* **116**, 1565–1568 (1969).
159. Chen, S., Gong, X. G., Walsh, A. & Wei, S.-H. Electronic structure and stability of quaternary chalcogenide semiconductors derived from cation cross-substitution of II-VI and I-III-VI₂ compounds. *Phys. Rev. B* **79**, 165201 (2009).
160. Walsh, A., Chen, S., Wei, S.-H. & Gong, X.-G. Kesterite thin-film solar cells: advances in materials modelling of Cu₂ZnSnS₄. *Adv. Energy Mater.* **2**, 400–409 (2012).
161. Chen, S. Y. et al. Compositional dependence of structural and electronic properties of Cu₂ZnSn(S,Se)₄ alloys for thin film solar cells. *Phys. Rev. B* **83**, 125201 (2011).
162. Wallace, S. K., Mitzi, D. B. & Walsh, A. The steady rise of kesterite solar cells. *ACS Energy Lett.* **2**, 776–779 (2017).
163. Wang, W. et al. Device characteristics of CZTSSe thin-film solar cells with 12.6% efficiency. *Adv. Energy Mater.* **4**, 1301465 (2014).
164. Bourdais, S. et al. Is the Cu/Zn disorder the main culprit for the voltage deficit in kesterite solar cells? *Adv. Energy Mater.* **6**, 1502276 (2016).
165. Chen, S., Walsh, A., Gong, X.-G. & Wei, S.-H. Classification of lattice defects in the kesterite Cu₂ZnSnS₄ and Cu₂ZnSnSe₄ earth-abundant solar cell absorbers. *Adv. Mater.* **25**, 1522–1539 (2013).
166. Chen, S. Y., Yang, J.-H., Gong, X. G., Walsh, A. & Wei, S.-H. Intrinsic point defects and complexes in the quaternary kesterite semiconductor Cu₂ZnSnS₄. *Phys. Rev. B* **81**, 245204 (2010).
167. Chen, S., Gong, X. G., Walsh, A. & Wei, S.-H. H. Defect physics of the kesterite thin-film solar cell absorber Cu₂ZnSnS₄. *Appl. Phys. Lett.* **96**, 021902 (2010).
168. Yoo, H. & Fauchet, P. Dielectric constant reduction in silicon nanostructures. *Phys. Rev. B* **77**, 115355 (2008).
169. Han, D. et al. Deep electron traps and origin of p-type conductivity in the earth-abundant solar-cell material Cu₂ZnSnS₄. *Phys. Rev. B* **87**, 155206 (2013).
170. Zhai, Y. T. et al. Structural diversity and electronic properties of Cu₂SnX₃ (X = S, Se): a first-principles investigation. *Phys. Rev. B* **84**, 075213 (2011).
171. Burton, L. A., Kumagai, Y., Walsh, A. & Oba, F. DFT investigation into the underperformance of sulfide materials in photovoltaic applications. *J. Mater. Chem. A* **5**, 9132–9140 (2017).
172. Schorr, S. The crystal structure of kesterite type compounds: a neutron and X-ray diffraction study. *Sol. Energy Mater. Sol. Cells* **95**, 1482–1488 (2011).
173. Parisi, M., Choubrac, L., Lafond, A., Guillot-Deudon, C. & Jobic, S. Solid-state NMR and Raman spectroscopy to address the structure of defects and the tricky issue of the Cu/Zn disorder in Cu-poor, Zn-rich CZTS materials. *Inorg. Chem.* **53**, 8646–8653 (2014).
174. Dimitrijevska, M., Fairbrother, A., Saucedo, E., Pérez-Rodríguez, A. & Izquierdo-Roca, V. Influence of compositionally induced defects on the vibrational properties of device grade Cu₂ZnSnSe₄ absorbers for kesterite based solar cells. *Appl. Phys. Lett.* **106**, 073903 (2015).
175. Schorr, S. Structural aspects of adamantine like multinary chalcogenides. *Thin Solid Films* **515**, 5985–5991 (2007).
176. Choubrac, L. et al. Multinuclear (⁶⁷Zn, ¹¹⁹Sn and ⁶⁵Cu) NMR spectroscopy — an ideal technique to probe the cationic ordering in Cu₂ZnSnS₄ photovoltaic materials. *Phys. Chem. Chem. Phys.* **15**, 10722–10725 (2013).
177. Scragg, J. J. S., Choubrac, L., Lafond, A., Ericson, T. & Platzner-Björkman, C. A low-temperature order-disorder transition in Cu₂ZnSnS₄ thin films. *Appl. Phys. Lett.* **104**, 041911 (2014).
178. Rey, G. et al. The band gap of Cu₂ZnSnS₄: effect of order-disorder. *Appl. Phys. Lett.* **105**, 112106 (2014).
179. Valentini, M. et al. Effect of the order-disorder transition on the optical properties of Cu₂ZnSnS₄. *Appl. Phys. Lett.* **108**, 211909 (2016).
180. Rudisch, K., Ren, Y., Platzner-Björkman, C. & Scragg, J. Order-disorder transition in B-type Cu₂ZnSnS₄ and limitations of ordering through thermal treatments. *Appl. Phys. Lett.* **108**, 231902 (2016).
181. Scragg, J. J. S. et al. Cu-Zn disorder and band gap fluctuations in Cu₂ZnSn(S,Se)₄: theoretical and experimental investigations. *Phys. Status Solidi B* **253**, 247–254 (2016).
182. Zawadzki, P., Zakutayev, A. & Lany, S. Entropy-driven clustering in tetrahedrally bonded multinary materials. *Phys. Rev. Appl.* **3**, 1–7 (2015).
183. Repins, I. L. et al. Indications of short minority-carrier lifetime in kesterite solar cells. *J. Appl. Phys.* **114**, 1–5 (2013).
184. Liu, F. et al. Nanoscale microstructure and chemistry of Cu₂ZnSnS₄/CdS interface in kesterite Cu₂ZnSnS₄ solar cells. *Adv. Energy Mater.* **6**, 1600706 (2016).
185. Hages, C. J. et al. Identifying the real minority carrier lifetime in nonideal semiconductors: a case study of kesterite materials. *Adv. Energy Mater.* **116**, 1700167 (2017).
186. Kim, S., Park, J.-S. & Walsh, A. Identification of killer defects in kesterite thin-film solar cells. *ACS Energy Lett.* **3**, 496–500 (2018).
187. Moller, C. K. Crystal structure and photoconductivity of caesium plumbobhalides. *Nature* **182**, 1436–1436 (1958).
188. Weber, D. $\text{CH}_3\text{NH}_3\text{PbX}_3$, a Pb(II)-system with cubic perovskite structure. *Z. Naturforsch. B* **33**, 1443–1445 (1978).
189. Kojima, A., Teshima, K., Shirai, Y. & Miyasaka, T. Organometal halide perovskites as visible-light sensitizers for photovoltaic cells. *J. Am. Chem. Soc.* **131**, 6050–6051 (2009).
190. Stranks, S. D. & Snaith, H. J. Metal-halide perovskites for photovoltaic and light-emitting devices. *Nat. Nanotechnol.* **10**, 391–402 (2015).
191. Walsh, A. Principles of chemical bonding and band gap engineering in hybrid organic–inorganic halide perovskites. *J. Phys. Chem. C* **119**, 5755–5760 (2015).
192. Brivio, F., Butler, K. T., Walsh, A. & Van Schilfgaarde, M. Relativistic quasiparticle self-consistent electronic structure of hybrid halide perovskite photovoltaic absorbers. *Phys. Rev. B* **89**, 155204 (2014).
193. Frost, J. M. & Walsh, A. What is moving in hybrid halide perovskite solar cells? *Acc. Chem. Res.* **49**, 528–535 (2016).
194. Yin, W.-J., Shi, T. & Yan, Y. Unusual defect physics in $\text{CH}_3\text{NH}_3\text{PbI}_3$ perovskite solar cell absorber. *Appl. Phys. Lett.* **104**, 063903 (2014).
195. Brandt, R. E., Stevanović, V., Ginley, D. S. & Buonassisi, T. Identifying defect-tolerant semiconductors with high minority-carrier lifetimes: beyond hybrid lead halide perovskites. *MRS Commun.* **5**, 265–275 (2015).
196. Walsh, A. & Zunger, A. Instilling defect tolerance in new compounds. *Nat. Mater.* **16**, 964–967 (2017).
197. Stoddard, R. J., Eickmeyer, F. T., Katahara, J. K. & Hillhouse, H. W. Correlation between photoluminescence and carrier transport and a simple *in situ* passivation method for high-bandgap hybrid perovskites. *J. Phys. Chem. Lett.* **8**, 3289–3298 (2017).
198. Onoda-Yamamoto, N., Matsuo, T. & Suga, H. Dielectric study of $\text{CH}_3\text{NH}_3\text{PbX}_3$ (X = Cl, Br, I). *J. Phys. Chem. Solids* **53**, 935–939 (1992).
199. Baumann, A. et al. Identification of trap states in perovskite solar cells. *J. Phys. Chem. Lett.* **6**, 2350–2354 (2015).
200. Yang, W. S. et al. Iodide management in formamidinium-lead-halide-based perovskite layers for efficient solar cells. *Science* **356**, 1376–1379 (2017).
201. Kim, G. Y. et al. Large tunable photoeffect on ion conduction in halide perovskites and implications for photodecomposition. *Nat. Mater.* **17**, 445–449 (2018).
202. Umari, P., Mosconi, E. & De Angelis, F. Relativistic GW calculations on $\text{CH}_3\text{NH}_3\text{PbI}_3$ and $\text{CH}_3\text{NH}_3\text{SnI}_3$ perovskites for solar cell applications. *Sci. Rep.* **4**, 4467 (2014).
203. Du, M.-H. Density functional calculations of native defects in $\text{CH}_3\text{NH}_3\text{PbI}_3$: effects of spin-orbit coupling and self-interaction error. *J. Phys. Chem. Lett.* **6**, 1461–1466 (2015).
204. Walsh, A., Scanlon, D. O., Chen, S., Gong, X. G. & Wei, S.-H. Self-regulation mechanism for charged point defects in hybrid-halide perovskites. *Angew. Chem. Int. Ed.* **54**, 1791–1794 (2015).
205. Mandel, G. Self-compensation limited conductivity in binary semiconductors. I. Theory. *Phys. Rev.* **134**, A1073–A1079 (1964).
206. Whalley, L. D., Crespo-Otero, R. & Walsh, A. H-Center and V-center defects in hybrid halide perovskites. *ACS Energy Lett.* **2**, 2713–2714 (2017).

207. Tasker, P. W. & Stoneham, A. M. An appraisal of the molecular model for the V_k centre. *J. Phys. Chem. Solids* **38**, 1185–1189 (1977).
208. Shluger, A. L., Puchin, V. E., Suzuki, T., Tanimura, K. & Itoh, N. Optical transitions of the H centers in alkali halides. *Phys. Rev. B* **52**, 4017–4028 (1995).
209. Zohar, A. et al. What is the mechanism of MAPbI₃ p-doping by I₂? Insights from optoelectronic properties. *ACS Energy Lett.* **2**, 2408–2414 (2017).
210. Hoke, E. T. et al. Reversible photo-induced trap formation in mixed-halide hybrid perovskites for photovoltaics. *Chem. Sci.* **6**, 613–617 (2015).
211. Mosconi, E. et al. Light-induced annihilation of Frenkel defects in organo-lead halide perovskites. *Energy Environ. Sci.* **9**, 3180–3187 (2016).
212. Grancini, G. et al. Role of microstructure in the electron–hole interaction of hybrid lead halide perovskites. *Nat. Photonics* **9**, 695–702 (2015).
213. Yang, T.-Y., Gregori, G., Pellet, N., Grätzel, M. & Maier, J. Significance of ion conduction in a organic–inorganic lead-iodide-based perovskite photosensitizer. *Angew. Chem. Int. Ed.* **54**, 7905–7910 (2015).
214. Mitzi, D. B., Wang, S., Feild, C. A., Chess, C. A. & Guloy, A. M. Conducting layered organic–inorganic halides containing <110>-oriented perovskite sheets. *Science* **267**, 1473–1476 (1995).
215. Savory, C. N., Walsh, A. & Scanlon, D. O. Can Pb-free halide double perovskites support high-efficiency solar cells? *ACS Energy Lett.* **1**, 949–955 (2016).
216. Zakutayev, A., Perry, N. H., Mason, T. O., Ginley, D. S. & Lany, S. Non-equilibrium origin of high electrical conductivity in gallium zinc oxide thin films. *Appl. Phys. Lett.* **103**, 232106 (2013).
217. Zhang, S. B., Wei, S.-H. & Zunger, A. Microscopic origin of the phenomenological equilibrium “doping limit rule” in n-type III–V semiconductors. *Phys. Rev. Lett.* **84**, 1232–1235 (2000).
218. Walukiewicz, W. Mechanism of Fermi-level stabilization in semiconductors. *Phys. Rev. B* **37**, 4760–4763 (1988).
219. Zunger, A. Practical doping principles. *Appl. Phys. Lett.* **83**, 57–59 (2003).
220. Wei, S.-H. Overcoming the doping bottleneck in semiconductors. *Comput. Mater. Sci.* **30**, 337–348 (2004).
221. Zhang, S. B., Wei, S.-H. & Zunger, A. A phenomenological model for systematization and prediction of doping limits in II–VI and I–III–V₂ compounds. *J. Appl. Phys.* **83**, 3192–3196 (1998).
222. Walsh, A. et al. Limits to doping of wide band gap semiconductors. *Chem. Mater.* **25**, 2924–2926 (2013).
223. Buckeridge, J. et al. Polymorph engineering of TiO₂: demonstrating how absolute reference potentials are determined by local coordination. *Chem. Mater.* **27**, 3844–3851 (2015).
224. Shi, L. & Wang, L.-W. Ab initio calculations of deep-level carrier nonradiative recombination rates in bulk semiconductors. *Phys. Rev. Lett.* **109**, 245501 (2012).
225. Alkauskas, A., Yan, Q., de Walle, C. G. & Van De Walle, C. G. First-principles theory of nonradiative carrier capture via multiphonon emission. *Phys. Rev. B* **90**, 17–27 (2014).
226. Mandelkorn, J. & Lambeck, J. H. Simplified fabrication of back surface electric field silicon cells and novel characteristics of such cells. *Sol. Cells* **29**, 121–130 (1990).
227. Lundberg, O., Bodegård, M., Malmström, J. & Stolt, L. Influence of the Cu(In, Ga)Se₂ thickness and Ga grading on solar cell performance. *Prog. Photovolt.* **11**, 77–88 (2003).
228. Lee, M., Ngan, L., Hayes, W., Sorensen, J. & Panchala, A. F. Understanding next generation cadmium telluride photovoltaic performance due to spectrum. *2015 IEEE 42nd Photovolt. Specialist Conference (PVSC)* <https://doi.org/10.1109/PVSC.2015.7356003>
229. Sinsermsuksakul, P. et al. Overcoming efficiency limitations of SnS-based solar cells. *Adv. Energy Mater.* **4**, 1400496 (2014).
230. Polizzotti, A. et al. Improving the carrier lifetime of tin sulfide via prediction and mitigation of harmful point defects. *J. Phys. Chem. Lett.* **8**, 3661–3667 (2017).
231. Shockley, W. & Queisser, H. J. Detailed balance limit of efficiency of p–n junction solar cells. *J. Appl. Phys.* **32**, 510–519 (1961).
232. Yu, L. & Zunger, A. Identification of potential photovoltaic absorbers based on first-principles spectroscopic screening of materials. *Phys. Rev. Lett.* **108**, 068701 (2012).
233. Blank, B., Kirchartz, T., Lany, S. & Rau, U. Selection metric for photovoltaic materials screening based on detailed-balance analysis. *Phys. Rev. Appl.* **8**, 024032 (2017).
234. Steirer, K. X. et al. Defect tolerance in methylammonium lead triiodide perovskite. *ACS Energy Lett.* **1**, 360–366 (2016).
235. Zakutayev, A. et al. Defect tolerant semiconductors for solar energy conversion. *J. Phys. Chem. Lett.* **5**, 1117–1125 (2014).
236. Hendon, C. H. et al. Electroactive nanoporous metal oxides and chalcogenides by chemical design. *Chem. Mater.* **29**, 3663–3670 (2017).
237. Ganose, A. M., Savory, C. N. & Scanlon, D. O. Beyond methylammonium lead iodide: prospects for the emergent field of ns² containing solar absorbers. *Chem. Commun.* **103**, 15729–15735 (2016).
238. Tan, Y. P., Povolotskyi, M., Kubis, T., Boykin, T. B. & Klimeck, G. Tight-binding analysis of Si and GaAs ultrathin bodies with subatomic wave-function resolution. *Phys. Rev. B* **92**, 085301 (2015).
239. Menéndez-Proupin, E., Amézaga, A. & Cruz Hernández, N. Electronic structure of CdTe using GGA+U^{SCF}. *Phys. B Condens. Matter* **452**, 119–123 (2014).
240. Park, J.-S., Yang, J.-H., Ramanathan, K. & Wei, S.-H. Defect properties of Sb- and Bi-doped CuInSe₂: the effect of the deep lone-pair s states. *Appl. Phys. Lett.* **105**, 243901 (2014).
241. Redinger, A. et al. Time resolved photoluminescence on Cu(In, Ga)Se₂ absorbers: distinguishing degradation and trap states. *Appl. Phys. Lett.* **110**, 122104 (2017).
242. Stranks, S. D. et al. Electron-hole diffusion lengths exceeding 1 micrometer in an organometal trihalide perovskite absorber. *Science* **342**, 341–344 (2013).
243. Yang, Y. et al. Comparison of recombination dynamics in CH₃NH₃PbBr₃ and CH₃NH₃PbI₃ perovskite films: influence of exciton binding energy. *J. Phys. Chem. Lett.* **6**, 4688–4692 (2015).
244. Shi, D. et al. Low trap-state density and long carrier diffusion in organolead trihalide perovskite single crystals. *Science* **347**, 519–522 (2015).
245. deQuilettes, D. W. et al. Photoluminescence lifetimes exceeding 8 μs and quantum yields exceeding 30% in hybrid perovskite thin films by ligand passivation. *ACS Energy Lett.* **1**, 438–444 (2016).
246. Poindexter, E. H. et al. Electronic traps and P_b centers at the Si/SiO₂ interface: band-gap energy distribution. *J. Appl. Phys.* **56**, 2844–2849 (1984).
247. Voronkov, V. V., Falster, R., Bothe, K., Lim, B. & Schmidt, J. Lifetime-degrading boron-oxygen centres in p-type and n-type compensated silicon. *J. Appl. Phys.* **110**, 063515 (2011).
248. Niewelt, T., Schön, J., Broisch, J., Warta, W. & Schubert, M. Electrical characterization of the slow boron oxygen defect component in Czochralski silicon. *Phys. Status Solidi RRL* **9**, 692–696 (2015).
249. Niewelt, T., Mágdefessel, S. & Schubert, M. C. Fast in-situ photoluminescence analysis for a recombination parameterization of the fast BO defect component in silicon. *J. Appl. Phys.* **120**, 085705 (2016).
250. Huang, B. et al. Origin of reduced efficiency in Cu(In, Ga)Se₂ solar cells with high ga concentration: alloy solubility versus intrinsic defects. *IEEE J. Photovolt.* **4**, 477–482 (2014).
251. Krysztopa, A., Igelson, M., Gütay, L., Larsen, J. K. & Aida, Y. Defect level signatures in CuInSe₂ by photocurrent and capacitance spectroscopy. *Thin Solid Films* **535**, 366–370 (2013).

Acknowledgements

The authors thank S.-H. Wei, K.J. Chang, A. Zunger, A.A. Sokol, C.R.A. Catlow, and C.G. van de Walle for illuminating discussions regarding defects in semiconductors. This project has received funding from the European Horizon 2020 Framework Programme for research, technological development and demonstration (Grant No. 720907); see STARCELL for further information. A.W. is supported by a Royal Society University Research Fellowship and the Leverhulme Trust, and J.P. is supported by a Royal Society Shower Fellowship.

Author contributions

All authors researched data for the article and contributed to the discussion of content. J.-S.P., S.K. and A.W. wrote the article, and Z.X. edited and reviewed the article prior to submission.

Competing interests

The authors declare no competing interests.

Publisher's note

Springer Nature remains neutral with regard to jurisdictional claims in published maps and institutional affiliations.

RELATED LINKS

SC-FERMI: <https://sourceforge.net/projects/sc-fermi/>

STARCELL: <http://www.starcell.eu>